

Base-Free and Bisphosphine Ligand Dialkylmanganese(II) Complexes as Precursors for Manganese Metal Deposition

Jeffrey S. Price, Preeti Chadha, and David J. H. Emslie*

Department of Chemistry and Chemical Biology, McMaster University, Hamilton, Ontario L8S 4M1, Canada

Supporting Information Placeholder

ABSTRACT: The solid state structures and the physical, solution magnetic, solid state magnetic, and spectroscopic (NMR and UV/Vis) properties of a range of oxygen- and nitrogen-free dialkylmanganese(II) complexes are reported, and the solution reactivity of these complexes towards H₂ and ZnEt₂ is described. The compounds investigated are [$\{\text{Mn}(\mu\text{-CH}_2\text{SiMe}_3)_2\}_\infty$] (**1**), [$\{\text{Mn}(\text{CH}_2\text{CMe}_3)(\mu\text{-CH}_2\text{CMe}_3)_2\}_2\{\text{Mn}(\mu\text{-CH}_2\text{CMe}_3)_2\text{Mn}\}$] (**2**), [$\text{Mn}(\text{CH}_2\text{SiMe}_3)_2(\text{dmpe})$] (**3**) (dmpe = 1,2-bis(dimethylphosphino)ethane), [$\{\text{Mn}(\text{CH}_2\text{CMe}_3)_2(\mu\text{-dmpe})\}_2$] (**4**), [$\{\text{Mn}(\text{CH}_2\text{SiMe}_3)(\mu\text{-CH}_2\text{SiMe}_3)_2(\mu\text{-dmpe})\}$] (**5**), [$\{\text{Mn}(\text{CH}_2\text{CMe}_3)(\mu\text{-CH}_2\text{CMe}_3)_2(\mu\text{-dmpe})\}$] (**6**), [$\{\text{Mn}(\text{CH}_2\text{SiMe}_3)(\mu\text{-CH}_2\text{SiMe}_3)_2(\mu\text{-dmpm})\}$] (**7**) (dmpm = bis(dimethylphosphino)methane), and [$\{\text{Mn}(\text{CH}_2\text{CMe}_3)(\mu\text{-CH}_2\text{CMe}_3)_2(\mu\text{-dmpm})\}$] (**8**). Syntheses for **1-4** have previously been published, but the solid state structures and most properties of **2-4** had not been described. Compounds **5** and **6**, with a 1:2 dmpe:Mn ratio, were prepared by reaction of **3** and **4** with base-free **1** and **2**, respectively. Compounds **7** and **8** were accessed by reaction of **1** and **2** with 0.5 or more equivalents of dmpm per manganese atom. An X-ray structure of **2** revealed a tetrametallic structure with two terminal and six bridging alkyl groups. In the solid state, bisphosphine-coordinated **3-8** adopted three distinct structural types: (a) monometallic [LMnR_2], (b) dimetallic [$\text{R}_2\text{Mn}(\mu\text{-L})_2\text{MnR}_2$], and (c) dimetallic [$\{\text{RMn}(\mu\text{-R})\}_2(\mu\text{-L})$] (L = dmpe or dmpm). Compound **3** exhibited particularly desirable properties for an ALD or CVD precursor, melting at 62–63 °C, subliming at 60 °C (5 mTorr) and showing negligible decomposition after 24 h at 120 °C. Comparison of variable temperature solution and solid state magnetic data provided insight into the solution structures of **2-8**. Solution reactions of **1-8** with H₂ yielded manganese metal, demonstrating the thermodynamic feasibility of the key reaction steps required for manganese(II) dialkyl complexes to serve, in combination with H₂, as precursors for metal ALD or pulsed-CVD. By contrast, the solution reactions of **1-8** with ZnEt₂ yielded a zinc-manganese alloy with an approximate 1:1 Zn:Mn ratio.

INTRODUCTION

Prominent methods for thin film deposition include electroplating, electroless deposition, physical vapor deposition (PVD), chemical vapor deposition (CVD), and atomic layer deposition (ALD).¹ Electroplating and electroless deposition are conducted in solution or a melt, whereas PVD relies upon evaporation or sputtering of the target material under vacuum, often using resistive or electron beam heating or bombardment by high energy particles, respectively. By contrast, CVD and ALD are vapor phase deposition techniques requiring at least one volatile molecular precursor molecule as a source of elements in the target thin film. In CVD, the target material is formed by thermal decomposition of the volatile molecular precursor upon contact with a heated substrate. By contrast, in ALD, a volatile molecular precursor is adsorbed on the surface of a heated substrate and the resulting monolayer is reacted with a volatile co-reactant (a molecular co-reactant in the case of thermal ALD, or plasma-generated atoms in the case of plasma-enhanced ALD) to

produce a sub-monolayer of the target material. Precursor and co-reactant pulses are separated by inert gas or vacuum purge steps, and the precursor pulse/purge/co-reactant pulse/purge sequence is repeated until a film of the desired thickness is obtained.²

Of the thin film deposition methods described above, thermal ALD is uniquely well suited to deposit the highly uniform and conformal ultra-thin films required in future microelectronic devices. For this reason, ALD is currently used to deposit HfO₂ in microprocessors, Al₂O₃ in Dynamic Random Access Memory, and ZnS in electroluminescent displays.³ Thermal metal ALD has been reported for the following late transition metals: Cu, Ni, Pd, Pt, Co, Rh, Ir, Fe, Ru and Os.⁴ However, reports of more electropositive early- or mid-transition metal ALD are scarce (*vide infra*), given that most ALD precursors contain a metal in a positive oxidation state, which must be reduced to the zero oxidation state for metal film deposition. ALD of moderately electropositive

tungsten has been achieved using WF_6 in combination with Si_2H_6 ,⁵ SiH_4 ,⁶ or B_2H_6 .^{6b,7} Furthermore, ALD of elemental chromium, which is significantly more electropositive ($\chi_{\text{Pauling}} = 1.66$)⁸ than tungsten, was recently reported by Winter using $[\text{Cr}(\text{OCMe}^t\text{BuCH}=\text{N}^t\text{Bu})_2]$ and $\text{BH}_3(\text{NHMe}_2)$. However, film growth was only observed on $\text{Ru}/\text{SiO}_2/\text{Si}$ substrates, a lengthy nucleation process was required, and film thickness plateaued at approx. 10 nm. Manganese ALD⁹ was also likely achieved using $[\text{Mn}_2(\text{OCMe}^t\text{BuCH}=\text{N}^t\text{Bu})_4]$ and $\text{BH}_3(\text{NHMe}_2)$, although only MnO_x was observed after air exposure, and the same substrate, nucleation and film growth restrictions that applied to Cr also applied to Mn.¹⁰ Cu-Mn alloy ALD has recently been reported using a combination of $[\text{Mn}_2(\text{OCMe}^t\text{BuCH}=\text{N}^t\text{Bu})_4] / \text{BH}_3(\text{NHMe}_2)$ and $[\text{Cu}(\text{dmap})_2] / \text{BH}_3(\text{NHMe}_2)$ cycles (dmap = 1-dimethylamino-2-propoxide).¹¹ Additionally, titanium ALD was recently accomplished using TiCl_4 in combination with 2-methyl-1,4-bis(trimethylsilyl)-2,5-cyclohexadiene or 1,4-bis(trimethylsilyl)-1,4-dihydropyrazine.¹²

We have previously investigated the use of metal alkyl complexes (e.g. ZnEt_2) as co-reactants for copper metal ALD,¹³ and in this work we set out to determine whether highly reactive electropositive transition metal alkyl complexes could exhibit the reactivity, volatility, and thermal stability suitable to effect electropositive metal deposition in combination with reagents such as H_2 or ZnEt_2 (hydrogen gas has previously been used as a co-reactant for ALD of Fe,¹⁴ Ru,¹⁵ Co,¹⁴ Ir,¹⁶ Ni,^{14,17} Pd,¹⁸ and Cu;^{14,19} ZnEt_2 has been used as a co-reactant for ALD of Cu²⁰).

As ALD precursors, electropositive metal alkyl complexes offer several potential advantages relative to coordination or cyclopentadienyl complexes: (a) the high reactivity of polar metal-alkyl bonds may provide access to low temperature reaction pathways for elemental metal deposition,²³ (b) the metal-nitrogen and metal-oxygen bonds typically encountered in coordination complexes can be avoided, precluding metal oxide or nitride formation, and (c) in reactions with H_2 , the byproducts are highly unreactive and volatile alkanes which should be readily eliminated from the growing film. Transition metal alkyl complexes have rarely been used as precursors for pulsed-CVD or ALD, although notable exceptions are $[\text{PtMe}_2(\text{COD})]$,²¹ and $[\text{Cp}'\text{PtMe}_3]$ ²² (COD = 1,5-cyclooctadiene, Cp' = methylcyclopentadienyl)

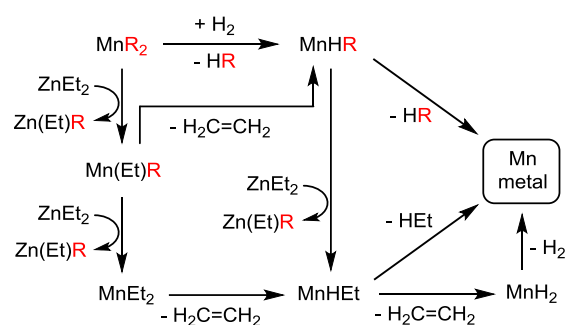
Manganese was selected as the metal of choice in the current work due to a Pauling electronegativity ($\chi_{\text{Pauling}} = 1.55$) lower than that of all transition metals in groups 5-12, with the exception of tantalum ($\chi_{\text{Pauling}} = 1.5$).⁹ Furthermore, manganese ALD is of interest since copper-manganese alloys can be used for self-formation of a MnSi_xO_y diffusion barrier at the interface between copper interconnect wiring and dielectric materials rich in silicon and oxygen.²⁴

Reactivity envisaged between a dialkylmanganese precursor and H_2 or ZnEt_2 is shown in Scheme 1. With H_2 , a mixed alkyl hydride complex (MnHR) should be accessible by σ -bond metathesis, or oxidative addition of H_2 followed by reductive elimination of HR . This mixed alkyl hydride complex can be expected to be particularly susceptible to HR reductive elimination for both thermodynamic and kinetic reasons,²⁵ leading to manganese metal deposition. With ZnEt_2 , stepwise alkyl exchange with MnR_2 would provide $\text{Mn}(\text{Et})\text{R}$ and then MnEt_2 , which can be expected to undergo rapid β -hydride elimination to form either MnHR or MnHET

respectively. MnHR is the same intermediate targeted in reactions with H_2 , and MnHET will decompose via either HET reductive elimination to form manganese metal, or β -hydride elimination to form MnH_2 ; an unstable species observed only in low temperature matrices.²⁶ While HR ($\text{R} = \text{CH}_2\text{EMe}_3$) is the only byproduct expected in reactions with H_2 , byproducts in the reactions with ZnEt_2 can include ZnEtR (or ZnR_2 ; not shown in Scheme 1), ethylene, HR , HET , and H_2 .

The aforementioned reactivity can only be utilized for manganese ALD or pulsed-CVD if a dialkylmanganese(II) precursor with an appropriate balance of thermal stability, volatility, and reactivity can be identified. The first neutral dialkylmanganese(II) complex, MnMe_2 , was reported by Beermann and Clauss over a half century ago, although the structure this compound, which explodes under the influence of shock or friction, remains unknown.²⁷ By contrast, Wilkinson *et al.* prepared homoleptic trimethylsilylmethyl, neopentyl, neophyl ($\text{CH}_2\text{CMe}_2\text{Ph}$),²⁸ and 1-adamantylmethyl²⁹ manganese(II) complexes with much greater stability due to increased steric bulk. X-ray crystal structures were reported for the trimethylsilylmethyl and neophyl complexes, which are polymeric and dimeric, respectively.^{28b,30} More recently, homoleptic benzyl,³¹ *o*- $\text{CH}_2\text{C}_6\text{H}_4\text{NMe}_2$,³² bis(trimethylsilyl)methyl,³³ tris(trimethylsilyl)methyl,³⁴ and $\text{C}(\text{SiMe}_3)_2(\text{SiMe}_2\text{NMe}_2)$ ³⁵ manganese(II) complexes have also been crystallographically characterized.

Scheme 1. Possible pathways for $\text{Mn}_{(s)}$ deposition using dialkylmanganese(II) complexes in combination with H_2 or ZnEt_2 co-reactants.



Dialkylmanganese(II) complexes have been coordinated to a wide variety of Lewis bases including PMe_3 ,³⁶ PEt_3 , PMe_2Ph , PMePh_2 , PCy_3 ,³⁷ *dmpe* (1,2-bis(dimethylphosphino)ethane),^{36b,38} pyridine,^{31,39} 2,2'-bipyridine (*bipy*),³¹ *TMEDA* (*N,N,N',N'*-tetramethylethylenediamine),²⁸ a bidentate diimine ligand (*N,N'*-bis(mesitylmethylene)-1,2-cyclohexanediamine),⁴⁰ sparteine,⁴¹ THF ,^{31,38b,42} *iPr}_2\text{NC}(\text{O})\text{CH}_2\text{Ph},⁴³ 1,4-dioxane,³⁹ and a carbene (1,3-bis(2,6-diisopropylphenyl)imidazole-2-ylidene),⁴⁴ although many of these complexes have not been structurally characterized. Dialkylmanganese(II) complexes with *o*-phenylenedimethylene (*o*- $\text{C}_6\text{H}_4(\text{CH}_2)_2$),^{36b} cyclohexyl and *tert*-butyl⁴⁵ alkyl groups have also been isolated in combination with supporting *dmpe* ligands.*

Herein we describe the synthesis of both new and previously reported dialkylmanganese(II) complexes (8 in total), detailed solution and solid state characterization, including single crystal X-ray diffraction, PXRD, NMR and UV-Visible spectroscopy, and variable temperature solution

state (Evans) and solid state (SQUID) magnetic measurements, evaluation of thermal stability and volatility, and solution reactivity studies with H_2 and $ZnEt_2$ leading to manganese metal and manganese-zinc alloy electroless deposition. This work targets base-free as well as dmpe- and dmpm- (bis(dimethylphosphino)methane-) coordinated bis(trimethylsilylmethyl)- and dineopentyl- manganese(II) complexes, since (a) they have fairly low molecular weights and do not contain aromatic groups, maximizing the potential for appreciable volatility, (b) they do not contain β -hydrogen atoms, imparting thermal stability, (c) they are free from oxygen or nitrogen donors, precluding manganese oxide or nitride deposition, and (d) the chelate effect will help to prevent phosphine ligand dissociation during sublimation. The base-free compounds²⁸ and the 1:1 MnR_2 :dmpe adducts^{36b} have previously been reported, but an X-ray crystal structure has only been reported for $[\{Mn(\mu-CH_2SiMe_3)_2\}_\infty]$.

RESULTS AND DISCUSSION

Synthesis and X-ray Crystal Structures

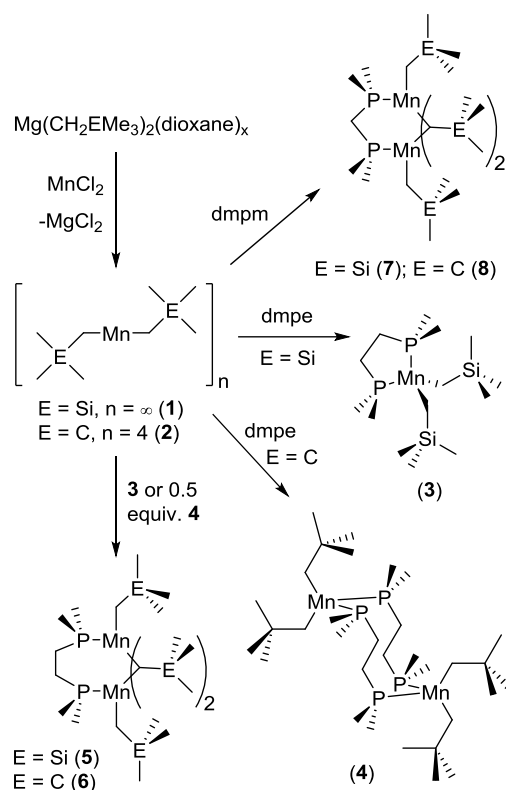
Base-free bis(trimethylsilylmethyl)manganese(II) (**1**) and dineopentylmanganese(II) (**2**) were prepared via the reactions of $MnCl_2$ with $MgR_2(\text{dioxane})_x$ ($R = CH_2SiMe_3$ or CH_2CMe_3 ; $x = 0.25-0.8$), following modifications of the literature procedures (Scheme 2).^{28b} The 1:1 Mn :dmpe (dmpe = 1,2-bis(dimethylphosphino)ethane) complexes, $[Mn(CH_2SiMe_3)_2(dmpe)]$ (**3**) and $[\{Mn(CH_2CMe_3)_2(\mu-dmpe)\}_2]$ (**4**), were also prepared as previously reported (Scheme 2),^{36b} while the 2:1 Mn :dmpe complexes, $[\{Mn(CH_2SiMe_3)(\mu-CH_2SiMe_3)_2(\mu-dmpe)\}_2]$ (**5**) and $[\{Mn(CH_2CMe_3)(\mu-CH_2CMe_3)_2(\mu-dmpe)\}_2]$ (**6**), were synthesized by addition of 1 equivalent of the corresponding base-free dialkylmanganese(II) precursor to **3** and **4**, respectively (Scheme 2). Compounds **1** and **2** reacted with bis(dimethylphosphino)methane (dmpm) to form exclusively $[\{Mn(CH_2SiMe_3)(\mu-CH_2SiMe_3)_2(\mu-dmpm)\}_2]$ (**7**) and $[\{Mn(CH_2CMe_3)(\mu-CH_2CMe_3)_2(\mu-dmpm)\}_2]$ (**8**), even when an excess of dmpm was added (Scheme 2).

Compound **4** is colourless, **3** is yellow, and **2** is dark brown, whereas **1** and **5-8** are red or black when crystalline, and pale pink when powdered. All eight compounds display high oxygen sensitivity, and were characterized by combustion elemental analysis, single crystal X-ray diffraction (except **1**),⁴⁶ PXRD on the bulk sample, ¹H NMR spectroscopy (except nearly insoluble **1**), UV/Vis spectroscopy (except nearly insoluble **1** and colourless **4**), and both SQUID and Evans solution magnetic measurements (except **1**); *vide infra*. Additionally, melting points and sublimation temperatures were determined, and thermal stability was assessed.

An X-ray structure has not previously been reported for base-free dineopentylmanganese(II) (**2**). However, Wilkinson *et al.* noted in 1976 that **2** is a tetramer in the solid state,^{28b} citing a personal communication from M. B. Hursthouse and P. Raithby.³⁰ Additionally, an electron diffraction study was reported for **2**, revealing a monometallic structure in the vapor phase.⁴⁷ In this work, dark brown X-ray quality crystals of **2** were obtained from hexanes at -30 °C, confirming a tetrametallic structure (Figure 1), with the two outer manganese atoms in a distorted trigonal planar geometry ($\Sigma(C-Mn(1)-C) = 359.82(6)^\circ$; $C-Mn(1)-C = 105.16(3)$, $122.62(3)$ and $132.04(4)^\circ$) and the inner manganese atoms in a

distorted tetrahedral geometry ($C-Mn(2)-C = 100.06(3)$ - $122.50(3)^\circ$). The only other neutral dialkylmanganese(II) complex known to contain a trigonal planar manganese center is $[\{Mn(CH_2CMe_2Ph)(\mu-CH_2CMe_2Ph)\}_2]$,^{28b,30,31} though it deviates more from planarity ($\Sigma(C-Mn-C) = 354.7(1)^\circ$) than complex **2**, likely due to an η^2 interaction between each manganese atom and the phenyl ring of a bridging CH_2CMe_2Ph group. The tetrametallic structure of **2** presumably differs from the polymeric structure of **1**^{28b} due to the increased steric demands of neopentyl versus trimethylsilylmethyl ligands.

Scheme 2. Synthesis of compounds 1-8.



Compound **2** has an inversion center between the central manganese atoms, and the terminal $Mn(1)-C(1)$ bond distance of $2.1211(9)$ Å is significantly shorter than the $Mn-C$ bonds to the bridging neopentyl ligands. For each bridging neopentyl group, one $Mn-C$ bond is approximately $0.1-0.2$ Å shorter than the other, with the short $Mn-C$ distances ranging from $2.213(1)$ to $2.232(1)$ Å, and long $Mn-C$ distances of $2.3265(7)$ to 3 -coordinate $Mn(1)$, and $2.3939(7)$ and $2.4092(9)$ Å to 4 -coordinate $Mn(2)$. Bridging alkyl groups in multimetallic manganese alkyl complexes in the literature also exhibit one short and one long $Mn-C$ bond,⁴⁸ as do all μ -alkyl manganese complexes in this work (*vide infra*). The $Mn(1)-Mn(2)$ and $Mn(2)-Mn(2')$ distances in **2** are $2.7022(4)$ and $2.7165(4)$ Å, which are almost 0.2 Å shorter than the $Mn-Mn$ distances previously reported for $[\{Mn(CH_2SiMe_3)_2\}_\infty]$ (**1**). Furthermore, the $Mn-C-Mn$ angles in **2** ($71.38(3)$ - $72.67(3)^\circ$) are approximately 5° more acute than those in **1**, while the $Mn-C$ distances are comparable.³¹ The $Mn-Mn$ distances in **2** lie between the sum of ionic (2.58 Å) and Van der Waals radii (4.10 Å),⁴⁹ and are within the range previously reported ($2.5-$

3.2 Å) for single Mn–Mn bonds in the vast majority of coordination and organometallic complexes.⁴⁸ However, they are longer than the shortest Mn–Mn distances in elemental manganese (2.26, 2.37 and 2.47 Å for α -, β - and γ -Mn, respectively).⁵⁰

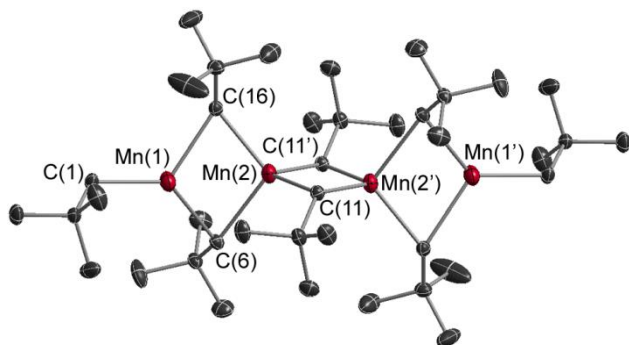


Figure 1. X-ray crystal structure for $[\{\text{Mn}(\text{CH}_2\text{CMe}_3)(\mu\text{-CH}_2\text{CMe}_3)_2\}_2\{\text{Mn}(\mu\text{-CH}_2\text{CMe}_3)_2\text{Mn}\}]$ (**2**). Hydrogen atoms are omitted for clarity, ellipsoids are set to 60 % (C) and 80 % (Mn). Bond distances (Å) and angles (°): Mn(1)···Mn(2) 2.7022(4), Mn(2)···Mn(2') 2.7165(4), Mn(1)–C(1) 2.1211(9), Mn(1)–C(6) 2.2322(9), Mn(2)–C(16) 2.232(1), Mn(2)–C(11) 2.213(1), Mn(1)–C(16) 2.3265(7), Mn(2)–C(6) 2.3939(7), Mn(2)–C(11') 2.4092(9), Mn(1)–C(6)–Mn(2) 71.38(3), Mn(1)–C(16)–Mn(2) 72.67(3), Mn(2)–C(11)–Mn(2') 71.85(3), C(1)–Mn(1)–C(6) 132.04(4), C(1)–Mn(1)–C(16) 122.62(3), C(6)–Mn(1)–C(16) 105.16(3).

X-ray quality crystals of the 1:1 Mn:dmppe complexes, $[\text{Mn}(\text{CH}_2\text{SiMe}_3)_2(\text{dmppe})]$ (**3**) and $[\{\text{Mn}(\text{CH}_2\text{CMe}_3)_2(\mu\text{-dmppe})\}_2]$ (**4**), were obtained from hexanes at -30 °C. Compound **3** (Figure 2) is monometallic with a tetrahedral geometry that is distorted due to the small bite angle of dmppe ($78.76(2)^\circ$ in **3**). By contrast, **4** (Figure 3) is dimetallic with bridging dmppe ligands and a Mn–Mn distance of 6.756(2) Å, which is far greater than the sum of the van der Waals radii. Compound **4** features tetrahedral manganese centers ($\text{X–Mn–X} = 94.79(2)\text{--}122.20(9)^\circ$; X = C or P) and a central 10-membered ring with a boat-chair-boat conformation, which is the dominant conformation of cyclododecane.^{51,52} An organometallic complex featuring a similar $\text{M}_2(\mu\text{-dppe})_2$ core (dppe = bis(diphenylphosphino)ethane) has been structurally characterized for Mo.⁵³ The Mn–P and Mn–C distances in **3** and **4** are unremarkable, ranging from 2.6241(9) to 2.6541(5) Å (Mn–P) and 2.1320(14) to 2.160(2) Å (Mn–C), similar to the Mn–P and Mn–C_{terminal} bond lengths in **1**, **2**, $[\text{Mn}(\text{CH}_2\text{Ph})_2(\text{PMe}_3)_2]$,^{36b} and $[\text{Mn}(\text{CH}_2\text{SiMe}_3)_2(\text{tmeda})]$ (tmeda = *N,N,N',N'*-tetramethyl-ethylenediamine).³⁹ By contrast, significantly longer Mn–P and Mn–C distances were reported for $[\text{Mn}\{\text{CH}(\text{SiMe}_3)_2\}_2(\text{dmppe})]$,^{38b} presumably due to greatly increased steric hindrance at the metal center.

Bright red X-ray quality crystals of $[\{\text{Mn}(\text{CH}_2\text{SiMe}_3)(\mu\text{-CH}_2\text{SiMe}_3)_2(\mu\text{-dmppe})\}_2]$ (**5**) were obtained at -30 °C from both toluene and hexanes. The unit cell for the structure obtained from toluene (Figure 4) contains three independent molecules, while the structure obtained from hexanes (Figure S36 in supporting information) has only one independent molecule in the unit cell. Black X-ray quality crystals of the neopentyl analogue, $[\{\text{Mn}(\text{CH}_2\text{CMe}_3)(\mu\text{-CH}_2\text{CMe}_3)_2(\mu\text{-dmppe})\}_2]$ (**6**) (Figure 5) were obtained from toluene at -30 °C. Both **5** and **6**

are dimetallic with tetrahedral manganese centers ($\text{C–Mn–X} = 94.4(1)\text{--}131.4(4)^\circ$; X = C or P) coordinated to one terminal alkyl group, two bridging alkyl groups, and one phosphorus atom of a bridging dmppe ligand. The terminal Mn–C distances in **5** and **6** [2.123(2)–2.141(5) Å in **5**; 2.160(6) and 2.18(1) Å in **6**] are shorter than the bridging Mn–C distances, and as in base-free **1** and **2**, each of the bridging alkyl groups is closer to one manganese atom than the other; the short Mn–C_{bridging} distances range from 2.183(2) to 2.211(4) Å in **5** and 2.252(5) to 2.27(1) Å in **6**, whereas the long Mn–C_{bridging} distances range from 2.362(2) to 2.379(4) Å in **5** and 2.300(9) to 2.342(6) Å in **6**.

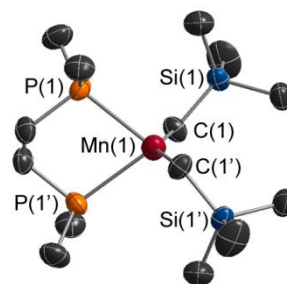


Figure 2. X-ray crystal structure for $[\text{Mn}(\text{CH}_2\text{SiMe}_3)_2(\text{dmppe})]$ (**3**). Hydrogen atoms are omitted for clarity, and ellipsoids are set to 50 % (C, P, Si) and 70 % (Mn). All carbon atoms in the dmppe ligand are disordered over two positions, and only the dominant conformation (69 %) is shown above. Bond distances (Å) and angles (°): Mn–C 2.1320(14), Mn–P 2.6541(5), P–Mn–P 78.76(2), C–Mn–C 144.34(9), P(1)–Mn–C(1) 108.59(5), P(1)–Mn–C(1') 98.89(4).

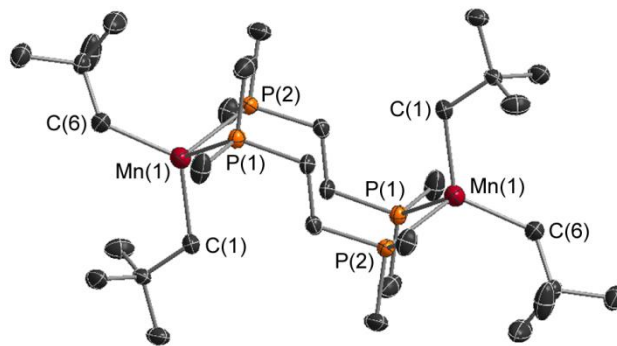


Figure 3. X-ray crystal structure for $[\{\text{Mn}(\text{CH}_2\text{CMe}_3)_2(\mu\text{-dmppe})\}_2]$ (**4**). Hydrogen atoms are omitted for clarity, and ellipsoids are set to 60 % (C, P) and 80 % (Mn). Bond distances (Å) and angles (°): Mn···Mn 6.756(2), Mn(1)–P(1) 2.6241(9), Mn(1)–P(2') 2.643(1), Mn(1)–C(1) 2.160(2), Mn(1)–C(6) 2.160(2), P(1)–Mn(1)–P(2) 94.79(2), C(1)–Mn(1)–C(6) 122.20(9), C(1)–Mn(1)–P(1) 104.25(7), C(6)–Mn(1)–P(1) 106.94(7), C(1)–Mn(1)–P(2) 119.20(7), C(6)–Mn–P(2) 105.25(7).

The Mn–P distances in **5** and **6** are similar and unexceptional. However, the Mn–Mn distances of 2.7177(6)–2.7322(6) Å in **5** are shorter than those in base-free **1** by over 0.15 Å, likely due to the tethering influence of the bridging bisphosphine ligand. The Mn–C–Mn angles in **5** [$72.88(7)\text{--}73.35(8)^\circ$] are also more acute than those in base-free **1** [$76.82(4)$ and $77.19(5)^\circ$], consistent with the shorter Mn–Mn

distance in the former compound. The Mn–Mn distance of 2.685(1) Å in **6** is less than 0.05 Å shorter than the corresponding distance in base-free **2**, but it is significantly shorter than the Mn–Mn distance in **5**. The Mn–C_{terminal} and average Mn–C_{bridging} distances (*vide supra*) are slightly longer in **6** than in **5**, and the Mn–C–Mn angles in **6** [71.5(2)–72.0(3)°] are slightly more acute than those in **5** (*vide supra*). These geometric trends mirror those observed for base-free **1** and **2**. An even shorter Mn–Mn distance of 2.616(5) Å, and a particularly acute Mn–C–Mn angle of 69.6(4)°, were previously reported for isostructural $[\{\text{MnCy}(\mu\text{-Cy})\}_2(\mu\text{-dmpe})]$ (Cy = cyclohexyl),⁴⁵ which features more sterically demanding and electron donating secondary alkyl groups.

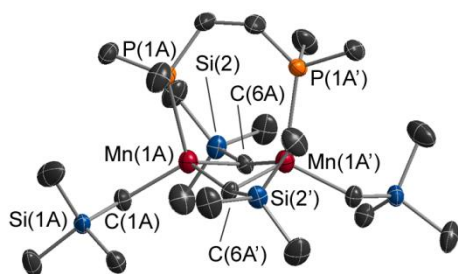


Figure 4. X-ray crystal structure for $[\{\text{Mn}(\text{CH}_2\text{SiMe}_3)(\mu\text{-CH}_2\text{SiMe}_3)\}_2(\mu\text{-dmpe})]$ (**5**) obtained by crystallization from toluene. Hydrogen atoms are omitted for clarity, and ellipsoids are set to 50 % (C, P, Si) and 70 % (Mn). The unit cell contains three independent and essentially isostructural molecules (A, B, and C), and only molecule A is shown. Bond distances (Å) and angles (°): Mn(1A)···Mn(1A') 2.7202(6), Mn(1B)···Mn(1B') 2.7177(6), Mn(1C)···Mn(1C') 2.7322(6), Mn(1A)–P(1A) 2.6007(9), Mn(1B)–P(1B) 2.5909(9), Mn(1C)–P(1C) 2.6020(9), Mn(1A)–C(1A) 2.123(2), Mn(1B)–C(1B) 2.137(2), Mn(1C)–C(1C) 2.136(2), Mn(1A)–C(6A) 2.183(2), Mn(1B)–C(6B) 2.200(2), Mn(1C)–C(6C) 2.208(2), Mn(1A)–C(6A') 2.366(2), Mn(1B)–C(6B') 2.370(2), Mn(1C)–C(6C') 2.362(2), Mn(1A)–C(6A)–Mn(1A') 73.34(7), Mn(1B)–C(6B)–Mn(1B') 72.88(7), Mn(1C)–C(6C)–Mn(1C') 73.35(8). See supporting information for bond distances and angles in the structure of **5** obtained from hexanes.

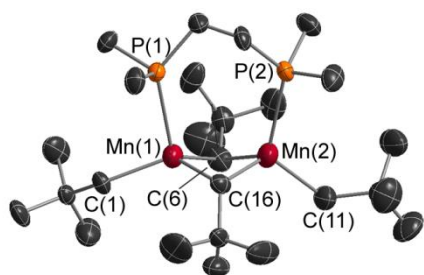


Figure 5. X-ray crystal structure for $[\{\text{Mn}(\text{CH}_2\text{CMe}_3)(\mu\text{-CH}_2\text{CMe}_3)\}_2(\mu\text{-dmpe})]$ (**6**). Hydrogen atoms are omitted for clarity, and ellipsoids are set to 50 % (C, P) and 70 % (Mn). Positions of all carbon atoms in three of the four neopentyl groups (C(1)–C(15)) are disordered over two positions. The figure shows only one position for each of the disordered groups (occupancy: 50 % for C1–C5, 82 % for C6–C10, and 87 % for C11–C15). Bond distances (Å) and angles (°): Mn(1)···Mn(2) 2.685(1), Mn(1)–P(1) 2.605(1), Mn(2)–P(2) 2.641(1), Mn(1)–C(1) 2.160(6), Mn(2)–C(11) 2.18(1), Mn(1)–C(16) 2.252(5), Mn(2)–C(6) 2.27(1), Mn(1)–C(6) 2.300(9), Mn(2)–C(16) 2.342(6), Mn(1)–C(6)–Mn(2) 72.0(3), Mn(1)–C(16)–Mn(2) 71.5(2).

Bright red X-ray quality crystals of $[\{\text{Mn}(\text{CH}_2\text{SiMe}_3)(\mu\text{-CH}_2\text{SiMe}_3)\}_2(\mu\text{-dmpm})]$ (**7**) were obtained from hexanes at –30 °C (Figure 6), revealing a dimetallic structure analogous to the structures of the 2:1 MnR₂:dmpe complexes, **5** and **6**. The Mn–Mn, Mn–C and Mn–P distances and Mn–C–Mn angles in **7** are very similar to those in **5**, although the dmpm ligand in **7** is bound less symmetrically than the dmpe ligand in **5** (the Mn–P distances in **7** differ by approx. 0.06 Å in **7**, compared with approx. 0.02 Å in **5**). The solid state structure of $[\{\text{Mn}(\text{CH}_2\text{CMe}_3)(\mu\text{-CH}_2\text{CMe}_3)\}_2(\mu\text{-dmpm})]$ (**8**) was also determined using crystals obtained (a) from hexanes at –30 °C, and (b) by slow evaporation of a hexanes solution at 20 °C (Figure S37; supporting info.). However, the quality of the both data sets was only suitable to establish connectivity, which is analogous to that of **7**.

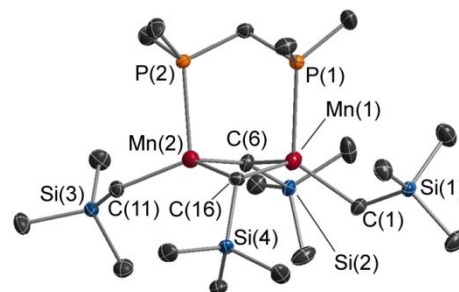


Figure 6. X-ray crystal structure for $[\{\text{Mn}(\text{CH}_2\text{SiMe}_3)(\mu\text{-CH}_2\text{SiMe}_3)\}_2(\mu\text{-dmpm})]$ (**7**). Hydrogen atoms are omitted for clarity, and ellipsoids are set to 50 % (C, P, Si) and 70 % (Mn). Bond distances (Å) and angles (°): Mn(1)···Mn(2) 2.7243(5), Mn(1)–P(1) 2.6584(5), Mn(2)–P(2) 2.6016(6), Mn(1)–C(1) 2.134(1), Mn(2)–C(11) 2.121(1), Mn(1)–C(6) 2.220(2), Mn(2)–C(16) 2.233(1), Mn(1)–C(16) 2.340(1), Mn(2)–C(6) 2.337(1), Mn(1)–C(6)–Mn(2) 73.38(5), Mn(1)–C(16)–Mn(2) 73.08(4).

The structures of **5** and **7** can also be compared with $[\{\text{Mn}(\text{CH}_2\text{SiMe}_3)(\mu\text{-CH}_2\text{SiMe}_3)(\text{PMe}_3)\}_2]$,^{36a} and an isostructural PET_3 complex, $[\{\text{Mn}(\text{CH}_2\text{SiMe}_3)(\mu\text{-CH}_2\text{SiMe}_3)(\text{PET}_3)\}_2]$,³⁷ which was structurally characterized in this work (Figure S35 in supporting information). Key differences are that the phosphine ligands in the PR_3 (R = Me or Et) complexes are *trans* to one another across the Mn–Mn axis, and the Mn–Mn distances (2.772(1) Å (R = Me) and 2.7937(3) Å (R = Et)) are 0.05 to 0.07 Å longer than those in **5** and **7**. Furthermore, the Mn–C–Mn angles in the monophosphine complexes (74.5(1)° for R=Me and 75.21(3)° for R=Et) are less acute than those in **5** and **7** (~73°), while Mn–P and Mn–C distances are comparable. These data highlight the substantial influence of the bidentate dmpe ligand on the relative orientation of the phosphorus donors, the Mn–Mn distance, and the Mn–C–Mn angle. The neopentyl complex, $[\{\text{Mn}(\text{CH}_2\text{CMe}_3)(\mu\text{-CH}_2\text{CMe}_3)(\text{PMe}_3)\}_2]$,³⁷ has also been reported, featuring an elongated Mn–Mn distance (2.718(3) Å) and statistically equivalent Mn–C–Mn angles (69.6(6)° and 71.0(6)°) relative to **6**.

NMR Spectroscopy and Magnetic Measurements

The ¹H NMR spectra of complexes **2–8** (Figure 7; C₆D₆; 500 MHz) show paramagnetically broadened and shifted peaks, between 5 and 60 ppm, with full width at half maximum

values from 1150 to 8200 Hz. Further spectra were collected in d^8 toluene between 186 K and room temperature (Figure 8 for **6**; supporting information for **2-5** and **7-8**). A spectrum was not collected for **1** due to insolubility in non-coordinating solvents.

Based on the solid-state structure of phosphine-free **2**, six ^1H NMR signals are predicted with integrations of 36H, 18H, 18H, 8H, 4H and 4H. However, it is not unreasonable to expect that the MnCH_2 signals would be broadened to the point at which they cannot be located, due to their proximity to the high spin d^5 metal centers; in this case, a total of three ^1H NMR signals would be observed. At room temperature, the ^1H NMR spectrum of **2** shows only a single broad ^1H NMR resonance, but at -32°C this peak splits into the expected three signals.

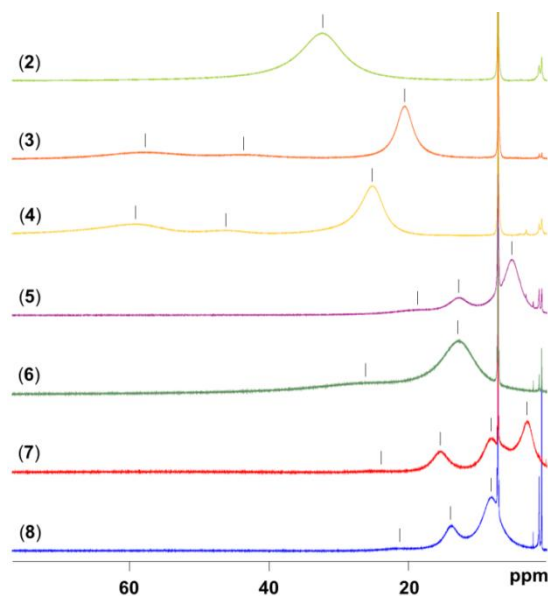


Figure 7. Room temperature ^1H NMR spectra for **2-8** (500 MHz, C_6D_6). Black tick marks indicate broad peaks associated with organomanganese(II) complexes, while the sharp signals are due to residual $\text{C}_6\text{D}_5\text{H}$ in the NMR solvent and trace hexanes.

The ^1H NMR spectra for dmpe complexes **3** and **4**,⁵⁴ which do not contain bridging alkyl groups, would be expected to give rise to three signals (18H, 12H and 4H not including MnCH_2 signals), whereas the ^1H NMR spectra for **5-8** should give rise to four signals (18H, 18H, 12H, 2H not including MnCH_2 signals). The expected number of signals was observed for **3**, **4** and **7** at 25°C , below 10°C for **5**, and below -28°C for **8**. For compound **6**, just two ^1H NMR signals were observed at room temperature, and at -15°C the largest of these signals split into two, yielding three broad peaks; the observation of just three signals (-15 to -80°C) in the spectrum for **6** is likely due to coincidental overlap of two signals (Figure 8). The increased number of signals in the low temperature ^1H NMR spectra of **2**, **5**, **6** and **8** may be attributed to (a) different temperature dependencies for overlapping paramagnetically shifted signals, or (b) decoalescence of signals that are averaged at room temperature due to exchange processes. For compound **8**, explanation ‘a’ is most likely on the basis of solution magnetic measurements (*vide infra*). By contrast, for compounds **2**, **5** and **6**, explanation ‘b’ seems

likely, given that solution magnetic measurements indicate that these tetrametallic or dimetallic complexes exist in equilibrium with other manganese-containing species in solution (*vide infra*).

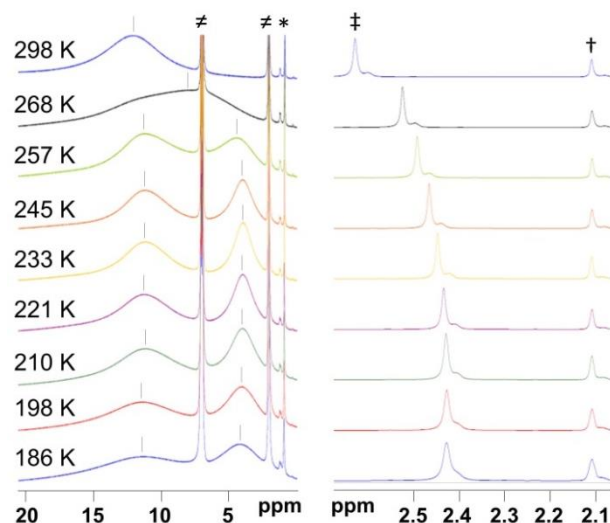


Figure 8. Left: ^1H NMR spectra for $[\{\text{Mn}(\text{CH}_2\text{CMe}_3)(\mu\text{-CH}_2\text{CMe}_3)\}_2(\mu\text{-dmpe})]$ (**6**) from 186 to 298 K (500 MHz, d^8 -toluene). Broad signals (|) are due to **6**, while sharp signals are due to residual d^7 -toluene solvent impurity (\neq) and hexanes (*). Right: Region of the ^1H NMR spectra used for Evans measurements between 186 and 298 K (500 MHz, 40:1 d^8 -toluene:toluene); the methyl group from external toluene (\dagger) is calibrated to 2.11 ppm, and the methyl group of internal toluene (\ddagger) is observed to shift with temperature. Shoulders to the right of the two toluene (C_7H_8) signals are the residual solvent signals due to d^7 -toluene, $\text{C}_6\text{D}_5(\text{CHD}_2)$.

Table 1. Room temperature solution and solid state magnetic data for **2-8**.

Complex	$\chi_{\text{M}(\text{corr})}$ per Mn centre in C_6D_6 at 298 K ($10^{-3} \text{ cm}^3/\text{mol}$)	$\chi_{\text{M}(\text{corr})}$ per Mn centre in the solid state at 300 K ($10^{-3} \text{ cm}^3/\text{mol}$)
2	4.2 ± 0.1^c	2.82 ± 0.03
3	13.6 ± 0.5 ($\mu_{\text{B}} = 5.71 \text{ BM} \pm 0.11$) ^d	14.0 ± 1.2 ($\mu_{\text{B}} = 5.8 \text{ BM} \pm 0.2$) ^a
4	14.4 ± 0.5 ($\mu_{\text{B}} = 5.87 \text{ BM} \pm 0.10$)	14.1 ± 0.1 ($\mu_{\text{B}} = 5.83 \text{ BM} \pm 0.03$) ^b
5	3.5 ± 0.3	3.48 ± 0.04
6	6.5 ± 0.3	3.30 ± 0.03
7	3.0 ± 0.2	3.24 ± 0.03
8	3.4 ± 0.1	3.35 ± 0.03

$\chi_{\text{M}(\text{corr})}$ = corrected molar magnetic susceptibility; μ_{B} = effective magnetic moment; θ = Weiss temperature; (a) $\theta = -0.6 \pm 0.1 \text{ K}$ for **3**; (b) $\theta = 0.04 \pm 0.06 \text{ K}$ for **4**. (c) Lit: 3.9 BM .^{25b} (d) Lit: 5.6 BM .^{36b}

Solid state and solution magnetic measurements were carried out on complexes **2-8** (Table 1). SQUID magnetic measurements have previously been reported for **1**, and show antiferromagnetic coupling/exchange between the manganese atoms.³⁹ SQUID magnetic measurements on **3**, which is monometallic, and **4**, which is a dimer with spatially separated manganese centres, show that both complexes obey the Curie-

Weiss law (Figure 9; 300 to 5 K), leading to effective magnetic moments (μ_B) of 5.8 ± 0.2 and 5.83 ± 0.03 BM, respectively, and magnetic susceptibilities ($\chi_{M(\text{corr})}$) of $14.0 \times 10^{-3} \pm 1.2 \times 10^{-3}$ and $14.08 \times 10^{-3} \pm 0.13 \times 10^{-3}$ cm³/mol of Mn at room temperature (for a high spin d⁵ metal center, the ideal values for μ_B and $\chi_{M(\text{corr})}$ are 5.92 BM and 14.6×10^{-3} cm³/mol, respectively). Compounds **3** and **4** are therefore paramagnetic with no antiferromagnetic exchange.

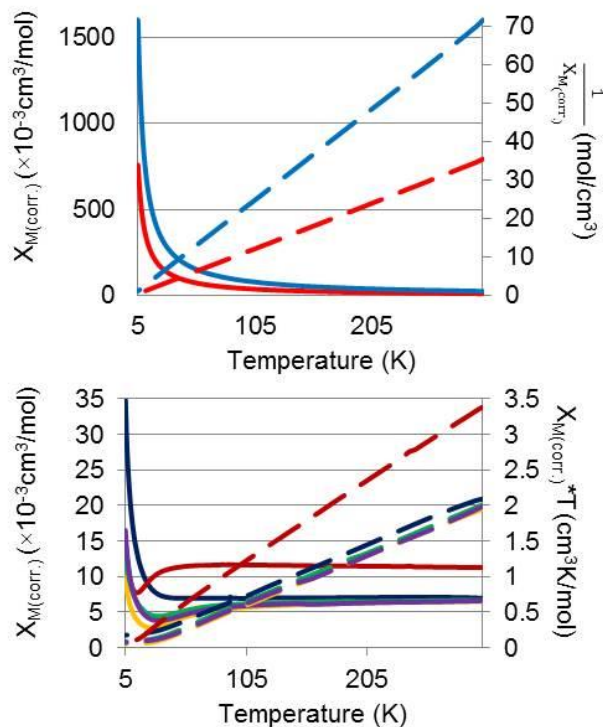


Figure 9. SQUID magnetic susceptibility data from 5 to 300 K. Top: $\chi_{M(\text{corr})}$ vs. T (solid lines) and $1/\chi_{M(\text{corr})}$ vs. T (dashed lines) for paramagnetic **3** (red) and **4** (blue). Bottom: $\chi_{M(\text{corr})}$ vs. T (solid lines) and $\chi_{M(\text{corr})} * T$ vs. T (dashed lines) for **2** (red), **5** (blue), **6** (purple), **7** (orange), and **8** (green), which feature antiferromagnetic interactions.

By contrast, the SQUID magnetic data (Figure 9) for complexes **2** and **5-8**, which feature Mn–Mn distances between 2.685(1) and 2.7322(6) Å, do not obey the Curie law, and are indicative of significant antiferromagnetic exchange/coupling between neighboring manganese centers (with paramagnetic impurity tails at low temperature). At room temperature, the magnetic susceptibility per manganese center is 2.82×10^{-3} cm³/mol for tetrametallic **2**, and ranges from 3.24×10^{-3} to 3.48×10^{-3} cm³/mol for bimetallic **5-8**; these values are far lower than that expected for a paramagnetic metal center with five unpaired d-electrons (14.6×10^{-3} cm³/mol). The variable temperature magnetic behaviour of **2** and **5-8** is qualitatively similar to that reported for polymeric **1**³⁹ and dimetallic $[\{\text{Mn}(\text{CH}_2\text{SiMe}_3)_2(\text{THF})\}_2]$,⁴² and for the latter compound, Lawrence *et. al.* concluded that the significant magnetism observed at low temperatures indicates an absence of Mn–Mn bonding, despite the short Mn–Mn distance of 2.7878(9) Å.⁴²

The SQUID magnetic susceptibility data for dinuclear **5-8** and tetranuclear **2** was fitted to an exchange expression (supporting information) for simple high spin Mn(II) systems using MAGMUN-4.1,⁵⁵ and the resulting fits (Table 2 and Figures S29-S33 in supporting information) are in good agreement with the experimental data. The resulting calculated g factors are close to 2.0, as expected for high spin organomanganese(II) complexes which lack an orbital contribution to the magnetic moment, and the exchange coupling constants (J) for **2** and **5-8** range from -107 to -117 cm⁻¹, indicative of strong antiferromagnetic coupling (J is an averaged value for compound **2**).

Table 2. Magnetic parameters determined by fitting an exchange expression to the SQUID magnetic susceptibility data for compounds **2** and **5-8**.

Compound ^a	Mean g-value	Intradimer J (cm ⁻¹)	ρ	θ (K)	100R
2 ^b	2.07 ± 0.01	-117 ± 1	0.005	2.4	0.71
5	2.12 ± 0.02	-112 ± 2	0.02	4.9	1.47
6	2.10 ± 0.02	-112 ± 2	0.01	1.1	1.03
7	2.07 ± 0.01	-109 ± 1	0.007	3.4	0.82
8	2.04 ± 0.03	-107 ± 2	0.011	5.1	1.06

J = exchange coupling constant; ρ = fraction paramagnetic impurity; θ = Weiss-like temperature correction; $R = [(\sum \chi_{\text{obs}} - \chi_{\text{calc}})^2 / (\sum \chi_{\text{obs}})^2]^{1/2}$; (a) The calculated temperature independent paramagnetism (TIP) is 0 cm³/mol for **2**, **6** and **7**, 4×10^{-5} cm³/mol for **5**, and 3×10^{-5} cm³/mol for **8**; (b) For **2**, J is average over the three Mn–Mn interactions present.

Solution state magnetic measurements were conducted using the Evans NMR method (Figure 8 and supporting information).⁵⁶ Measurements were taken at room temperature for all complexes (in a 40:1 mixture of C₆D₆:C₆H₆), and between 298 and 186 K for **2** and **5-7** (in a 40:1 mixture of d⁸-toluene:toluene). Complexes **3** and **4**, which are monometallic or feature well-separated manganese centers, have room temperature solution effective magnetic moments of 5.71 BM and 5.87 BM, respectively, which are very close to the theoretical value of 5.92 BM, and are statistically equivalent to the solid state effective magnetic moments. Dmpm complexes **7** and **8** gave rise to statistically identical solution and solid state magnetic susceptibilities at room temperature, indicating that the solid state structures of **7** and **8** remain intact in solution. Additionally, variable temperature Evans magnetic measurements on compound **7** (Figure 10; 298 to 186K) yielded magnetic susceptibility values that are statistically equivalent to those from SQUID measurements over the same temperature range.

By contrast, the solution magnetic susceptibilities for base-free **2** and dimetallic **6** are significantly higher than the solid state values (although they are still much lower than those expected in the absence of antiferromagnetic exchange). For dimetallic **6**, the solution magnetic susceptibility values decreased as the temperature was lowered, until an asymptote was reached at a value corresponding to that from solid state SQUID measurements; compound **5** showed analogous behavior, but with a much less pronounced change in magnetic susceptibility (Figures 9 and 10). This behavior is consistent with a solution equilibrium (significant above 245 K for **5**, and above 210 K for **6**) between the dimetallic solid state structures and entropically favored paramagnetic species; most

likely mononuclear $[\text{Mn}(\text{CH}_2\text{EMe}_3)_2(\text{dmpe})]$ [$\text{E} = \text{Si}$ (**3**) or C (**4**)] and base-free “ $\text{Mn}(\text{CH}_2\text{EMe}_3)_2$ ”. Our inability to directly observe the proposed minor solution species by variable temperature ^1H NMR spectroscopy is consistent with both the low concentrations of these species in solution, the broadness of the observed ^1H NMR signals, and the likelihood of rapid exchange between these species and **5** and **6**, especially at the upper end of the temperature range.

Unlike the solution magnetic susceptibility data for complexes **5** and **6**, the solution magnetic susceptibility of base-free **2** increased as the temperature was reduced and did not reach a plateau (Figure 10), moving increasingly further from the solid state magnetic susceptibility value of $2.82 \times 10^{-3} \text{ cm}^3/\text{mol}$ of Mn. This increase in magnetic susceptibility is indicative of an equilibrium that shifts at lower temperature towards species with weaker antiferromagnetic coupling than is observed in tetrametallic **2**. Above room temperature, the magnetic susceptibility of the solution (per manganese atom) continued to decrease towards the solid state value, but magnetic measurements were not accessible above 60°C ($\chi_{\text{M}(\text{corr})} = 3.8 \times 10^{-3} \text{ cm}^3/\text{mol}$) due to slow decomposition of solutions of **2** above this temperature.

Physical Properties of 1-8

Melting points ranging from 62 to 176°C were measured for **1-8** in a flame sealed glass capillary under an atmosphere of argon (Table 3). All complexes were found to melt without noticeable decomposition (determined visually and by ^1H NMR spectroscopy and/or PXRD after cooling to room temperature) if the temperature was reached quickly ($5^\circ\text{C}/\text{min}$), with the exception of **6** which showed minor decomposition. Importantly, the melting points of **3** and **4** match those reported by Wilkinson *et al.*,^{36b} confirming that the originally reported complexes were 1:1 Mn:dmpe complexes as proposed, rather than 2:1 complexes.

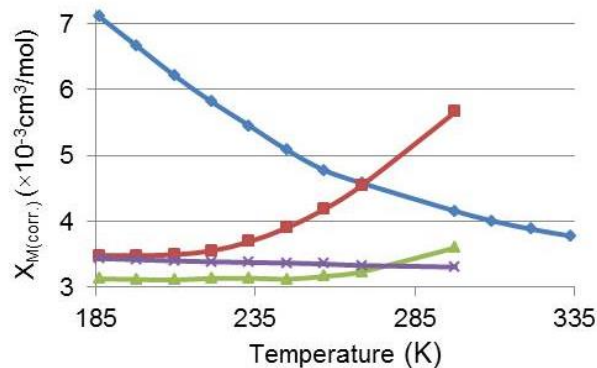


Figure 10. Solution magnetic susceptibilities per mole of Mn calculated from Evans measurements at various temperatures for $[\{\text{Mn}(\text{CH}_2\text{CMe}_3)(\mu\text{-CH}_2\text{CMe}_3)_2\}_2\{\text{Mn}(\mu\text{-CH}_2\text{CMe}_3)_2\text{Mn}\}]$ (**2**) (blue diamonds), $[\{\text{Mn}(\text{CH}_2\text{SiMe}_3)(\mu\text{-CH}_2\text{SiMe}_3)_2(\mu\text{-dmpe})\}]$ (**5**) (green triangles), $[\{\text{Mn}(\text{CH}_2\text{CMe}_3)(\mu\text{-CH}_2\text{CMe}_3)_2(\mu\text{-dmpe})\}]$ (**6**) (red squares), and $[\{\text{Mn}(\text{CH}_2\text{SiMe}_3)(\mu\text{-CH}_2\text{SiMe}_3)_2(\mu\text{-dmpm})\}]$ (**7**) (purple ‘x’ symbols).

Base-free $[\{\text{Mn}(\mu\text{-CH}_2\text{SiMe}_3)_2\}_n]$ (**1**), though very thermally stable (rapid decomp. 195°C), is not especially volatile (sublim. at $150\text{-}160^\circ\text{C}$; 5 mTorr). This low volatility can be explained by the polymeric nature of **1** in the solid

state. By contrast, $[\{\text{Mn}(\text{CH}_2\text{CMe}_3)(\mu\text{-CH}_2\text{CMe}_3)_2\}_2\{\text{Mn}(\mu\text{-CH}_2\text{CMe}_3)_2\text{Mn}\}]$ (**2**), which exists as a monomer in the vapor phase,⁴⁷ sublimed at 90°C (5 mTorr), but was more than 50% decomposed after 24h at 110°C . The remaining complexes, **3-8**, sublimed between 60 and 135°C at 5 mTorr , although **5** underwent extensive decomposition during sublimation, and **6** and **8** decomposed slowly at the sublimation temperature (Table 3). The 1:1 MnR₂:dmpe complexes, monometallic **3** and dimetallic **4**, exhibited the most promising volatility/thermal stability characteristics for possible applications in ALD or CVD, subliming at 60 and 80°C , respectively, with negligible decomposition after 24h at 120 and 110°C , respectively. Furthermore, **3** has a melting point of $62\text{-}63^\circ\text{C}$, so would be a liquid at the delivery temperature in a typical ALD or CVD experiment.

Table 3. Physical properties of complexes **1-8**.

Complex	m.p. ($^\circ\text{C}$)	Sublimation Temp. at 5 mTorr ($^\circ\text{C}$)	Thermal Decomp. Data ($^\circ\text{C}$) ^a
1	151-153 (lit. 98) ^{28b}	150-160 (lit. 150) ³⁹	195 (rapid decomp.)
2	99-102	90 (lit. 100) ^{28b}	110 (> 50 % after 24 h)
3	62-63 (lit. 62-64) ^{36b}	60	120 (v. little over 24 h)
4	132 (lit. 132-133) ^{36b}	80	120 (complete after 5-6 hours)
5	145-146	115-135 (decomp. products sublime)	120 (complete after 5-6 hours)
6	149-151.5 (part. decomp.)	110	110 (visible after 2-3 hours)
7	176	100	120 (v. little over 24 h)
8	161.5-165	100-120	110 (v. little over 24 h)

(a) Amount of decomposition assessed visually and by ^1H NMR spectroscopy and/or PXRD after cooling to room temperature.

Reactions with Hydrogen and Diethylzinc

Solutions of complexes **2-8**, or a slurry of **1**, were placed under 2 atm. of H_2 in an aromatic solvent, the reactions were monitored by ^1H NMR spectroscopy (Figures S46-S55 in supporting information), and insoluble products were characterized using PXRD (Figures S64-S65 in supporting information). Reactions took place between 25 and 120°C (Table 4), and in each case, a clear colourless or very pale beige solution was formed with a metallic-looking silver-grey mirror on the walls of the NMR tube (Scheme 3), or in one case (complex **1**) a precipitate of black powder. The diamagnetic reaction byproducts were tetramethylsilane or neopentane, accompanied by dmpe or dmpm in the case of compounds **3-8** (Scheme 3). The deposited solid was identified as manganese metal by PXRD. Additionally, conducting the reactions of **3** and **5** with H_2 in the presence of hexaethylbenzene as an internal NMR standard yielded exactly two and four equivalents of SiMe_4 , respectively,⁵⁷ illustrating complete removal of the alkyl groups from manganese. The appearance of the deposited films is also consistent with metallic manganese.

Table 4. Reaction conditions and by-products for: (i) the solution reactions of **1-8** with H₂ yielding Mn metal (determined by PXRD), and (ii) solution reactions of **1-8** with ZnEt₂ to deposit a 1:1 Mn/Zn alloy (determined by PXRD, and in some cases XPS; accompanied by Zn metal deposition in the reaction of **2** with ZnEt₂).

Complex	T _{reaction with H₂} (°C) / time (h)	H ₂ reaction by-products ^b	T _{reaction with ZnEt₂} (°C) / time (h)	ZnEt ₂ reaction by-products ^{a,b}
1	120 / 48	SiMe ₄	25 / 12	C ₂ H ₆ , C ₂ H ₄ , SiMe ₄ , ZnRX
2	25 / 72	CMe ₄	25 / 12	C ₂ H ₆ , C ₂ H ₄ , CMe ₄ , ZnRX
3	120 / 24	SiMe ₄ , dmpe	60 / 1	C ₂ H ₆ , C ₂ H ₄ , 9 ^d , SiMe ₄ , u.p. ^c
4	70 / 216 (or 100 / 24)	CMe ₄ , dmpe	25 / 72	C ₂ H ₆ , C ₂ H ₄ , 9 ^d , ZnRX
5	120 / 4	SiMe ₄ , 3	25 / 48	C ₂ H ₆ , C ₂ H ₄ , 9 ^d , SiMe ₄ , ZnRX,
6	25 / 168 (or 60 / 1)	CMe ₄ , 4	25 / 12	C ₂ H ₆ , C ₂ H ₄ , 9 ^d , ZnRX, u.p. ^c
7	120 / 4	SiMe ₄ , dmpm, u.p. ^c	90 / 0.5	C ₂ H ₆ , C ₂ H ₄ , ZnRX, dmpm
8	100 / 4	CMe ₄ , dmpm	95 / 1	C ₂ H ₆ , C ₂ H ₄ , ZnRX, dmpm

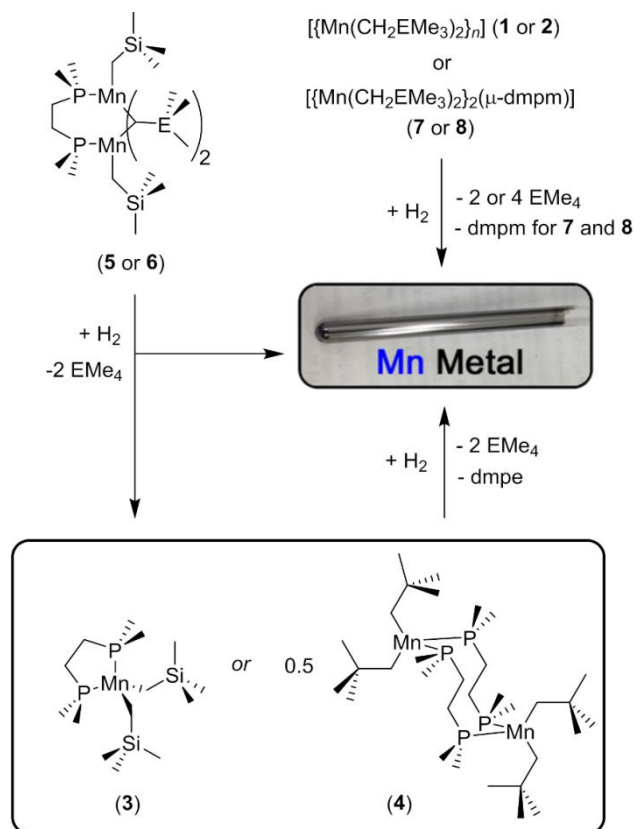
(a) R = CH₂EMe₃; X = Et or R; E = C or Si. (b) By-products identified by ¹H NMR spectroscopy. (c) u.p. = unidentified product. (d) Compound **9** is [MnH(C₂H₄)(dmpe)₂].⁶⁰

Polymeric complex **1** was the least reactive towards hydrogen, requiring several days at 120 °C to react completely, most likely due to very low solubility. By contrast, highly soluble tetrametallic **2** reacted to completion within three days at room temperature; **2** is far more reactive than **1** and **3-8**, likely due to the presence of 3-coordinate manganese centers. Complexes **3** and **4**, which contain one equivalent of dmpe per manganese center, showed low reactivity towards H₂; the reaction with **3** was only complete after 12 hours at 120 °C, and the reaction with **4** was complete after 24 hours at 100 °C. Dimetallic **5** and **6**, which contain half an equivalent of dmpe per manganese centre, reacted with H₂ to form **3** or **4**, accompanied by tetramethylsilane or neopentane and manganese metal. Complete consumption of **5** required 4.5 hours at 120 °C,⁵⁸ and the analogous reaction with **6** proceeded over a week at room temperature. The similarity in the reaction conditions required for consumption of **6** and **2** supports the proposal (*vide supra*) that in solution, **6** exists in equilibrium with **2** and **4** (*i.e.* H₂ likely reacts with **2** that is in equilibrium with **6** in solution, leaving unreacted **4**). Compounds **7** and **8** reacted with H₂ over the course of 4 hours at 120 °C and 100 °C, respectively. However, unlike the dmpe analogues (**5** and **6**), compounds **7** and **8** reacted with H₂ to provide manganese metal without formation of an observable monometallic intermediate. A general trend for **1-8** is the greater reactivity of the neopentyl complexes towards H₂.

Overall, the reactions of the dialkylmanganese(II) complexes and their bisphosphine adducts with H₂ highlight the utility of metal alkyl complexes for electropositive metal deposition, demonstrating the thermodynamic feasibility of key reaction steps en route to manganese deposition. In solution, base-free **2** and dmpe complex **6** displayed the highest reactivity. However, solution reaction temperatures

may not be of direct relevance to thermal ALD, given that adsorption to the surface of the growing thin film during ALD is likely to result in phosphine dissociation and/or formation of surface-bound species with coordination geometries and steric environments which differ significantly from those in the intact precursor complex.

Scheme 3. Reactions of **1-8** with H₂ in benzene or toluene.

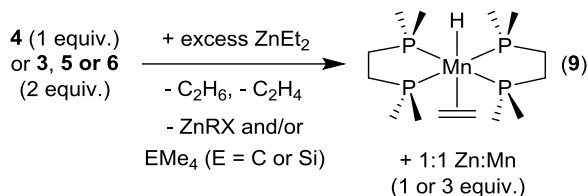


Complexes **1-8** were also reacted with 1-3 equivalents of ZnEt₂ (per Mn) in C₆D₆ (**2-8**) or d⁸-toluene (**1**) in a sealed NMR tube, the reactions were monitored by ¹H and/or ³¹P NMR spectroscopy (Figures S56-S63 in supporting information), and precipitated solids were characterized by PXRD and in some cases XPS (Figures S66-S71 in supporting information). Complexes **1-2** and **4-6** reacted completely over 12-72 hours at room temperature, whereas **3** required heating for 1 hour at 60 °C, and dmpm complexes **7** and **8** required heating at 90-95 °C for 30-60 minutes. In each of these reactions, a silver-coloured mirror was deposited onto the walls of the NMR tube, and ethane, ethylene and ZnX(CH₂EMe₃) (X = Et or CH₂EMe₃; E = Si or C) were released, accompanied in some cases by a small amount of EMe₄ (E = Si or C); H₂ formation was not observed. Compounds **7** and **8** released free dmpm,⁵⁹ whereas dmpe compounds **3-6** formed [MnH(C₂H₄)(dmpe)₂] (**9**)⁶⁰ (0.5 equiv. per Mn in **3-4** and 0.25 equiv. per Mn in **5-6**; Scheme 4), and free dmpe was not liberated.

The reactivity of **5** and **6** with ZnEt₂ is greater than that of **3** and **4**, respectively, implying that **3** and **4** are not formed as intermediates in the reactions of **5** and **6** with ZnEt₂, in contrast to the analogous reactions with H₂ (*vide supra*). The

aforementioned manganese(I) hydride compound, diamagnetic $[\text{MnH}(\text{C}_2\text{H}_4)(\text{dmpe})_2]$ (**9**), was first prepared by Wilkinson *et al.* via the reactions of manganese dihalides with MgEt_2 ,⁴⁵ and may be formed in this work by bi-molecular HR reductive elimination from manganese dihydride and manganese hydrido/alkyl centers, or comproportionation between a manganese dihydride species and elemental manganese (or an unobserved zero-valent manganese species formed en route to manganese metal).

Scheme 4. Reactions of dmpe complexes **3-6** with ZnEt_2 ($\text{R} = \text{CH}_2\text{EMe}_3$; $\text{X} = \text{Et}$ or R ; $\text{E} = \text{C}$ or Si) in benzene.



By PXRD, the insoluble product from the reactions of **1-8** with ZnEt_2 was a 1:1 manganese-zinc alloy,⁶¹ accompanied by zinc metal in the case of **2**. The presence of both zinc and manganese was further confirmed by XPS on representative samples ($\text{Zn:Mn} = 0.68 : 1$ for **2** and $1.32 : 1$ for **7**). Elemental zinc deposition could potentially occur via hydride transfer from a manganese hydride intermediate to a dialkyl zinc compound, leading to a zinc hydrido/alkyl species with very limited thermal stability; the only isolated zinc hydrido hydrocarbyl compounds contain extremely large aryl groups {e.g. $\text{R} = (\text{C}_6\text{H}_3-2,6-(\text{C}_6\text{H}_3-2,6-i\text{Pr}_2)_2$,⁶² $\text{C}_6\text{H}_3-2,6-(\text{C}_6\text{H}_2-2,4,6-i\text{Pr}_3)_2$, and $\text{C}_6\text{H}_2-2,6-(\text{C}_6\text{H}_2-2,4,6-i\text{Pr}_3)_2-4-\text{SiMe}_3$ }⁶³}, although ZnHMe has been observed in an argon matrix⁶⁴ and spectroscopically in the gas phase.^{65,66}

SUMMARY AND CONCLUSION

In the solid state, dineopentylmanganese(II) (**2**) is tetrametallic with two terminal alkyl groups and six bridging alkyl groups. The outer manganese centres are trigonal planar, whereas the inner manganese centres are tetrahedral. Dmpe complexes of bis(trimethylsilylmethyl)manganese(II) and dineopentylmanganese(II) adopt three distinct structural types: monometallic $[\text{LMnR}_2]$ (**3**), dimetallic $[\text{R}_2\text{Mn}(\mu\text{-L})_2\text{MnR}_2]$ (**4**), and dimetallic $[\{\text{RMn}(\mu\text{-R})\}_2(\mu\text{-L})]$ (**5-6**). By contrast, dmpm only yielded $[\{\text{RMn}(\mu\text{-R})\}_2(\mu\text{-L})]$ complexes (**7-8**). All polymetallic complexes feature doubly bridging alkyl groups with one long and one short Mn–C bond, and the neopentyl complexes exhibit more acute Mn–C–Mn angles and shorter Mn–Mn distances than trimethylsilylmethyl analogues.

All complexes have non-zero magnetic susceptibilities between 300 and 5 K. Both $[\text{Mn}(\text{CH}_2\text{SiMe}_3)_2(\text{dmpe})_2]$ (**3**) and $[\{\text{Mn}(\text{CH}_2\text{CMe}_3)_2(\mu\text{-dmpe})\}_2]$ (**4**) obey the Curie-Weiss law, whereas tetrametallic dineopentylmanganese(II) (**2**) and $[\{\text{RMn}(\mu\text{-R})\}_2(\mu\text{-L})]$ ($\text{L} = \text{dmpe}$ (**5-6**) or dmpm (**7-8**)) engage in strong antiferromagnetic coupling with J values from -107 to -117 cm^{-1} . Comparison of solution and solid state magnetic data indicates that the structures of the dmpm complexes (**7** and **8**) are maintained in solution, whereas the $[\{\text{RMn}(\mu\text{-R})\}_2(\mu\text{-dmpe})]$ complexes (**5** and **6**) exist in equilibrium at 25

$^\circ\text{C}$ with species with a higher average magnetic susceptibility; most likely $[(\text{dmpe})\text{MnR}_2]$ and “ MnR_2 ”. However, the solution magnetic susceptibilities of **5** and **6** decreased with decreasing temperature until an asymptote was reached, consistent with the presence of only **5** or **6** in solution at low temperature. In contrast, the magnetic susceptibility (per Mn) of dineopentylmanganese(II) (**2**) almost doubled as the temperature was reduced from 335 to 185 K, implying that the tetrametallic solid state structure is in equilibrium with species which exhibit less effective antiferromagnetic coupling and are favored at lower temperatures.

The two compounds without bridging alkyl groups (**3** and **4**) exhibited the most desirable thermal stability and volatility for ALD or CVD applications, and all CH_2SiMe_3 derivatives exhibited slightly increased thermal stability relative to CH_2CMe_3 analogues; monometallic **3** was the most promising, melting at $62\text{-}63 \text{ }^\circ\text{C}$, subliming at $60 \text{ }^\circ\text{C}$ (5 mTorr), and undergoing negligible decomposition after 24 h at $120 \text{ }^\circ\text{C}$.

Solution reactions of **1-8** with H_2 yielded manganese metal with elimination of 2 equiv. of HR ($\text{R} = \text{CH}_2\text{EMe}_3$; in all cases, neopentyl complexes displayed higher reactivity towards H_2 than trimethylsilylmethyl analogues), demonstrating the thermodynamic feasibility of the key reaction steps required for manganese(II) dialkyl complexes to serve, in combination with H_2 , as precursors for metal ALD or pulsed-CVD. By contrast, the solution reactions of **1-8** with ZnEt_2 yielded a zinc-manganese alloy with an approximate 1:1 Zn:Mn ratio, eliminating ethane and ethylene, accompanied by dmpm, $[\text{MnH}(\text{C}_2\text{H}_4)(\text{dmpe})_2]$ (**9**), EMe_4 and/or ZnXR ($\text{R} = \text{CH}_2\text{EMe}_3$; $\text{X} = \text{Et}$ or R). ALD/pulsed-CVD studies using **3**, **4**, and recently reported $[(\text{allyl}^{\text{TMS}_2})\text{Mn}\{\text{C}(\text{SiMe}_3)_3\}(\text{PMe}_3)]$ ⁶⁷ in combination with H_2 are in progress, and will be reported in due course.

EXPERIMENTAL SECTION

General Details. An argon-filled MBraun UNIlab glove box equipped with a $-30 \text{ }^\circ\text{C}$ freezer was employed for the manipulation and storage of all oxygen- and moisture-sensitive compounds. Air-sensitive preparative reactions were performed on a double-manifold high-vacuum line equipped with a two stage Welch 1402 belt-drive vacuum pump (ultimate pressure 1×10^{-4} torr) using standard techniques.⁶⁸ The vacuum was measured periodically using a Kurt J. Lesker 275i convection enhanced Pirani gauge, and residual oxygen and moisture was removed from the argon stream by passage through an Oxisorb-W scrubber from Matheson Gas Products. Commonly utilized specialty glassware included a swivel frit assembly, thick walled flasks equipped with Teflon stopcocks, J-Young or Wilmad-LabGlass LPV NMR tubes, Wilmad-LabGlass LPV EPR tubes, and Starna 1-Q-10/GS UV-Vis-NIR cells with spectroil far-UV quartz windows (transparent from 170 nm to 2700 nm), quartz to pyrex graded seals and Teflon stopcocks. Where indicated, a Branson 2510 ultrasonic bath was used to sonicate reaction mixtures. A VWR Clinical 200 Large Capacity Centrifuge (with 28° fixed-angle rotors that hold $12 \times 15 \text{ mL}$ or $6 \times 50 \text{ mL}$ tubes, and in combination with VWR high-performance polypropylene conical centrifuge tubes) located within a glove box was used where indicated.

Anhydrous diethyl ether was purchased from Aldrich, hexanes and toluene were purchased from Caledon, and

deuterated solvents were purchased from ACP Chemicals. Hexanes and toluene were initially dried and distilled at atmospheric pressure from sodium/benzophenone and sodium, respectively. All solvents were stored over an appropriate drying agent (diethyl ether, toluene, *d*₈-toluene, C₆D₆ = Na/Ph₂CO; hexanes = Na/Ph₂CO/tetraglyme) and introduced to reactions or solvent storage flasks via vacuum transfer with condensation at -78 °C.

Dmpe, dmpm, trimethylsilylmethylmagnesium chloride solution (1.0 M in diethyl ether), and 1,4-dioxane were purchased from Sigma-Aldrich. Manganese dichloride, neopentyl chloride, and diethyl zinc (min. 95 % in Sure-Pak cylinder) were purchased from Strem Chemicals. Argon and hydrogen gas were purchased from PraxAir. Bis(trimethylsilylmethyl)magnesium⁶⁹ and dineopentylmagnesium,^{28b} and were prepared according to the literature, though a slight excess of 1,4-dioxane was used leading to between 0.25 (trimethylsilylmethyl) and 0.8 (neopentyl) equivalents of 1,4-dioxane in the products. Bis(trimethylsilylmethyl)manganese(II)³⁹ was prepared according to literature procedures, though the reactant Bis(trimethylsilylmethyl)magnesium contained 0.25 equivalents of 1,4-dioxane. $[\{\text{Mn}(\text{CH}_2\text{SiMe}_3)(\mu\text{-CH}_2\text{SiMe}_3)(\text{PEt}_3)_2\}]$ was prepared as previously described.³⁷

NMR spectroscopy (¹H, ¹³C, and ³¹P{¹H}) was performed on Bruker DRX-500, AV-200 and AV-600 spectrometers. Spectra were obtained at 298 K unless otherwise indicated. All ¹H NMR spectra were referenced relative to SiMe₄ through a resonance of the proteo impurity of the solvent used: C₆D₆ (δ 7.16 ppm) and toluene-*d*₈ (δ 2.08 ppm, 6.97 ppm, 7.01 ppm, and 7.09 ppm). Also, all ¹³C NMR spectra were referenced relative to SiMe₄ through a resonance of the trace ¹³C in the solvents: C₆D₆ (δ 128.06 ppm) and toluene-*d*₈ (δ 20.43, 125.13, 127.96, 128.87, and 137.48 ppm). The ³¹P NMR spectra were referenced using an external standard of 85 % H₃PO₄ in D₂O (0.0 ppm). Various impurities (normally solvents) were identified by comparing to the tables of NMR chemical shifts of common impurities prepared by Karen Goldberg et. al.⁷⁰ Evans NMR measurements were conducted on the Bruker DRX-500 spectrometer in a manner described in the supporting information, and values are the average of two independent experiments. For **2**, $\chi_{[\text{M}(\text{corr})]}$ values above and below room temperature were collected using two different sets of samples; the values from 298 to 335 K were adjusted to give the same room temperature value by correcting the mass used from 8.3 to 8.6 mg, which is within the error of the mass balance.

Combustion elemental analyses were performed on a Thermo EA1112 CHNS/O analyzer. Samples for elemental analysis (typically 1-4 mg) were packed and sealed in pre-weighed 3 × 6 mm smooth wall tin capsules inside the glovebox. After removal from the glovebox, these capsules were packed into 5 × 8 mm pressed aluminum capsules containing approximately 10 mg of V₂O₅.

Single-crystal X-ray crystallographic analyses were performed on crystals coated in Paratone oil and mounted on a SMART APEX II diffractometer with a 3 kW sealed-tube Mo generator and SMART6000 CCD detector in the McMaster Analytical X-Ray (MAX) Diffraction Facility. Numerical absorption corrections were applied by face-indexing and a further semi-empirical absorption correction was applied using redundant data. Raw data was processed using XPREP (as part

of the APEX v2.2.0 software), and solved by direct methods (SHELXS-97).⁷¹ The structure was completed by difference Fourier synthesis and refined with full-matrix least-squares procedures based on *F*². In all cases, non-hydrogen atoms were refined anisotropically and hydrogen atoms were generated in ideal positions and then updated with each cycle of refinement. Powder X-ray diffraction experiments were performed on a Bruker D8 Advance powder diffractometer with Cu K α radiation ($\lambda = 0.154$ nm) operated at 40 kV and 40 mA. Powders were packed in 0.5 mm o.d. special glass (SG; wall thickness 0.01 mm) capillary tubes for X-ray diffraction (purchased from Charles Supper Co.) and sealed by inverting to submerge the open end in a pool of Apiezon H-grease within the glovebox. Calculated powder patterns were generated from the low-temperature single crystal data (for complexes **2-8**) and a file downloaded from the Cambridge Crystallographic Database (for complex **1**)³⁹ using Mercury. Experimental powder diffractograms were generated and viewed using Gadds, Powdercell, Crystal Sleuth, Diffrac.eva, Topaz, and PANalytical HighScore.

UV/Vis spectra were obtained on a Cary 50 UV/Visible Spectrometer using 10 mM to 10 μ M solutions in hexanes. Melting points were measured on a DigiMelt SRS MPA 160 melting point apparatus; between 1 and 2 mg of each sample was flame-sealed in a thin glass tube under an atmosphere of argon. X-Ray photoelectron spectra were collected on either a Thermo Scientific Thetaprobe or a K-Alpha (Thermo Scientific, E. Grinstead, UK) both of which are located at the University of Toronto. A monochromated Al K-Alpha was used with a spot size of 400 μ m. An initial survey spectrum was collected at low energy resolution for composition, as well as the high energy resolution spectrum of the Zn 2p, Zn Aug, and Mn 2p regions. SQUID measurements were collected on a Quantum Design MPMS between 5 K and 300 K at applied fields ranging from 100 Oe (for most) to 10 000 Oe (for complexes **3** and **6**). Roughly 50 mg of sample was placed in a sealed sample rod assembly for transport of air-sensitive samples into the magnetometer (with the exception of **3**, where between 2.9 and 3.4 mg of sample was placed in a flame-sealed glass capillary).

Thermal stability data was obtained by sealing approx. 10 mg of powder under argon in a flask with a teflon valve. This flask was heated to the desired temperature for 24 hours and then cooled to room temperature for visual inspection as well as PXRD and/or ¹H NMR spectroscopy. When 'very little' is used to describe the extent of decomposition, this indicates that the compound darkened in colour, but that decomposition was not observed by PXRD or ¹H NMR spectroscopy.

Complexes **1-8** are exceptionally air sensitive, as is diethyl zinc, and the phosphines dmpm and dmpe are malodorous. Therefore, all syntheses were conducted under an atmosphere of argon, in a fume hood where necessary.

$[\{\text{Mn}(\text{CH}_2\text{CMe}_3)(\mu\text{-CH}_2\text{CMe}_3)_2\}_2\{\text{Mn}(\mu\text{-CH}_2\text{CMe}_3)_2\text{Mn}\}]$
(**2**). MnCl₂ (2 g, 15.9 mmol) was suspended in 20 mL of diethyl ether. Mg(CH₂CMe₃)₂(1,4-dioxane)_{0.8} (4.9 g, 20.7 mmol) was dissolved separately in 40 mL of diethyl ether and added dropwise to the MnCl₂ suspension over 20 minutes. The reaction was stirred at room temperature for four days with regular sonication. The resulting yellow/light brown suspension was centrifuged to remove MgCl₂, and the solvent was removed from the resulting solution *in vacuo*. Crude **2** was extracted into toluene forming a dark brown solution, and

the solvent was again removed *in vacuo*. The remaining solid was recrystallized from hexanes (~ 10 mL) at -30 °C to afford large brown crystals. The mother liquors were then concentrated and maintained for several days at -30 °C to afford a 2nd batch of crystals; the total yield was 60 % (1.88 g). Note that on one occasion, a white solid was obtained rather than the expected dark brown solid. This solid was likely the Et₂O or 1,4 dioxane adduct of dioneopentylmanganese(II), and was converted to pure **2** by extended exposure to dynamic vacuum. Compound **2** was found to sublime at 90 °C (5 mTorr) and to melt between 99 and 102 °C. X-ray quality crystals were obtained from hexanes at -30 °C. ¹H NMR (C₆D₆): 32.6 ppm. (d⁸-toluene, 298 K): 28.2 (d⁸-toluene, 233 K): 14.9, 28.9, 65.9 ppm. Vis: λ_{max} = 464 nm. Anal. Found (Calcd): C, 60.18 (60.90); H, 10.75 (11.24).

[Mn(CH₂SiMe₃)₂(dmpe)] (3) and [Mn(CH₂CMe₃)₂(μ-dmpe)]₂ (4). The 1:1 dialkylmanganese(II):dmpe adducts were prepared according to literature procedures.^{36b} Complex **3** was purified by sublimation (60 °C at 5 mTorr) to a bright yellow powder, and complex **4** was purified by recrystallization from hexanes to afford a white powder (**4** also sublimed cleanly between 80 °C and 100 °C at 5 mTorr). X-ray quality crystals of **3** and **4** were obtained from hexanes at -30 °C. Complex **3**: ¹H NMR (C₆D₆): 20.6, 44.0, 58.1 ppm. (d⁸-toluene, 298 K): 20.6, 43.4, 56.4 ppm. (d⁸-toluene, 233 K): 26.2, 76 (v. broad) ppm. Anal. Found (Calcd): C, 44.16 (44.31); H, 10.36 (10.09). Complex **4**: ¹H NMR (C₆D₆): 25.2, 46.3, 59.1 ppm. (d⁸-toluene, 298 K): 25.1, 45.6, 56.5 ppm. (d⁸-toluene, 233 K): 30.6, 67 (v. broad) ppm. Anal. Found (Calcd): C, 56.02 (55.32); H, 11.11 (11.03).

[Mn(CH₂SiMe₃)(μ-CH₂SiMe₃)₂(μ-dmpe)] (5). [Mn(μ-CH₂SiMe₃)₂]_∞ (**1**) (67.1 mg, 0.294 mmol of Mn) and [Mn(CH₂SiMe₃)₂(dmpe)] (**3**) (110.9 mg, 0.292 mmol) were dissolved in toluene at -78 °C. The resulting light orange solution was stirred for 1 hour at -78 °C and 3 hours at room temperature before solvent was removed *in vacuo*. The resulting powder was dissolved in 1 mL of hexanes, centrifuged to remove a white solid impurity, and maintained at -30 °C for several days to produce orange/red crystals, which when crushed yielded an orange powder (87.2 mg; 49 % yield). The product was found to melt cleanly between 145 and 146 °C when heated quickly. ¹H NMR (C₆D₆): 5.2, 12.7, 19 (v. broad) ppm. (d⁸-toluene, 298 K): 5.2, 12.7, 19 (v. broad) ppm. (d⁸-toluene, 233 K): 2.5, 7.6, 12.1, 19 (v. broad) ppm. Vis: λ_{max} = 477 nm. Anal. Found (Calcd): C, 43.01 (43.40); H, 9.58 (9.93).

[Mn(CH₂CMe₃)(μ-CH₂CMe₃)₂(μ-dmpe)] (6). Tetrametallic **2** (110mg, 0.14 mmol) and dimetallic **4** (200 mg, 0.29 mmol) were dissolved in 5 mL of toluene. The solution was stirred overnight at room temperature, and then maintained at -30 °C for several days to obtain black crystals. The mother liquor was concentrated and maintained at -30 °C for several days to obtain a second batch of crystals, leading to a total yield of 92 % (279 mg). The product sublimed at 110 °C at 5 mTorr and melted with some decomposition between 149 and 151.5 °C. ¹H NMR (C₆D₆): 12.8, 26 (v. broad) ppm. (d⁸-toluene, 298 K): 12.2, 25 (v. broad) ppm. (d⁸-toluene, 233 K): 4.0, 11.3, 31 (v. broad) ppm. Vis: λ_{max} = 486 nm. Anal. Found (Calcd): C, 57.06 (57.34); H, 11.23 (11.11).

[Mn(CH₂SiMe₃)(μ-CH₂SiMe₃)₂(dmpm)] (7). A suspension of [Mn(μ-CH₂SiMe₃)₂]_∞ (**1**) (119 mg, 0.52 mmol per Mn) in toluene (20 mL) was cooled to -78 °C. A solution of dmpm

(180 mg, 1.3 mmol) in toluene (2 mL) was then added dropwise, and after stirring for 30 minutes at -78 °C and 1.5 hours at room temperature, the suspension turned to a clear orange solution. The solvent was then removed *in vacuo* and the solid was extracted with hexanes. After centrifuging to remove residual solid, the clear red hexanes solution was maintained at -30 °C for several days. The resulting red crystals were of X-ray quality. Crushing the crystals afforded a light pink powder (99 mg; 52 % yield). Complex **7** sublimed cleanly at 100 °C (5 mTorr) and melted without significant decomposition when heated rapidly to 176 °C (note: partial melting commenced at 160 °C). ¹H NMR (C₆D₆): 3.1, 7.9, 15.5, 24 (v. broad) ppm. (d⁸-toluene, 298 K): 3.1, 7.7, 15.4, 25 (v. broad) ppm. (d⁸-toluene, 233 K): 2.5, 8.4, 15.4, 25 (v. broad) ppm. Vis: λ_{max} = 476 nm. Anal. Found (Calcd): C, 42.24 (42.40); H, 9.86 (9.83).

[Mn(CH₂CMe₃)(μ-CH₂CMe₃)₂(dmpm)] (8). dmpm (220 mg, 1.61 mmol) was added to a solution of tetrametallic **2** (310 mg, 0.39 mmol) in a 4:1 mixture of hexanes and toluene (10 mL total). The reaction mixture was stirred for 24 hours after which time the solvent was removed *in vacuo* to give a brown powder (70 % yield). Both recrystallization over days at -30 °C from saturated hexanes, and slow evaporation of hexanes yielded thin red needles. The product sublimed between 100 and 120 °C at 5 mTorr and melted without decomposition between 161 and 165 °C. ¹H NMR (C₆D₆): 8.1, 13.8, 21 (v. broad) ppm. (d⁸-toluene, 298 K): 8.1, 13.8, 21 (v. broad) ppm. (d⁸-toluene, 233 K): 4.9, 11.4, 12.9, 19 (v. broad) ppm. Vis: λ_{max} = 481 nm. Anal. Found (Calcd): C, 56.16 (56.60); H, 11.34 (11.02).

Reactions with H₂(g). Approx. 10 mg of each complex was dissolved in approx. 1 mL of C₆D₆ (with the exception of [Mn(μ-CH₂SiMe₃)₂]_∞) which was suspended in approx. 1 mL of d₈-toluene). The resulting solution (or suspension) was placed in a thick-walled NMR tube with a J-Young Teflon valve and was freeze-pump-thawed (x 3). The NMR tube was then placed under an atmosphere of hydrogen gas, cooled to -95 °C using a liquid nitrogen-acetone bath, sealed at this low temperature, and warmed to room temperature to provide approx. 1.7 atm. of hydrogen gas. Reactions were then observed by ¹H NMR spectroscopy as a function of time and temperature. Upon reaction completion, gases were removed by exposing to dynamic argon, and solutions were decanted. Shiny metallic mirrors on the walls of the NMR tubes were sonicated into around 2 mL of toluene (rarely, the mirrors were physically scratched into suspension). The resulting silver-black powder was then washed twice with 5 mL of toluene and once with 5 mL of hexanes, dried *in vacuo*, and examined by PXRD.

Reactions with diethyl zinc. These reactions were conducted in a manner analogous to those with H₂, with the following modifications: Approx. 10-15 mg of each manganese complex was used, and rather than addition of H₂, 1-3 equivalents of neat diethyl zinc was added to the solution (or suspension) in the NMR tube within the glovebox, and the Teflon valve was immediately closed to ensure that volatile reaction byproducts did not escape. The resulting silver mirrors were sonicated to yield silver-black powders (in most cases pyrophoric) which were examined by PXRD, as well as XPS in some cases.

ASSOCIATED CONTENT

Supporting Information

CIF files, Crystallographic details, X-ray structures of **5** (crystallized from toluene), **8**, and $[\{\text{Mn}(\text{CH}_2\text{SiMe}_3)(\mu\text{-CH}_2\text{SiMe}_3)(\text{PEt}_3)\}_2]$, UV/Visible spectra, SQUID data and fits, Evans magnetic measurement data, ^1H NMR spectra of pure products and reactions with H_2 and ZnEt_2 , PXRD and XPS data.

AUTHOR INFORMATION

Corresponding Author

* D.J.H.E.: tel, 905-525-9140; fax, 905-522-5209;
e-mail, emslied@mcmaster.ca.

Notes

The authors declare no competing financial interests.

ACKNOWLEDGEMENTS

D.J.H.E. thanks Intel Corporation for funding through Semiconductor Research Corporation (SRC). We are grateful to Paul Dube and Dr. Yuriy Mozharivskiy for assistance with SQUID operation and analysis, Dr. Hilary Jenkins, Dr. Jim Britten, and Victoria Jarvis for assistance with single crystal and powder X-ray diffraction, Megan Fair for running combustion elemental analysis, Allen Paucic for assistance in determining T_1 relaxation times and attempting DOSY NMR spectroscopy, and Dr. Rana Sodhi (Surface Interface Ontario) for running XPS on selected samples.

REFERENCES

- (a) Smith, D. L., *Thin Film Deposition: Principles and Practice*, McGraw Hill, USA, 1995. (b) *Modern Electroplating*, 5th Ed., Schlesinger M. Ed., John Wiley & Sons: Hoboken, New Jersey, 2014.
- (a) So long as the amount of precursor and co-reactant delivered to the surface is sufficient to ensure complete reaction and maximum surface coverage, film thickness will depend only on the number of precursor/purge/co-reactant/purge cycles, even within high aspect ratio features. This is termed self-limiting growth, and if self-limiting growth cannot be achieved, the deposition method is pulsed-CVD, rather than ALD. (b) For the remainder of this paper, ALD will refer exclusively to thermal ALD.
- (a) Ritala, M.; Niinistö, J. Atomic Layer Deposition. In *Chemical Vapour Deposition: Precursors, Processes and Applications*; Jones, A. C., Hitchman, M. L., Eds.; Royal Society of Chemistry, 2009; Ch. 4, pp 158-271. (b) Kääriäinen, T.; Cameron, D.; Kääriäinen, M.-L.; Sherman, A. *Atomic Layer Deposition: Principles, Characteristics and Nanotechnology Applications*; Scrivener Publishing: Salem, Massachusetts, 2013. (c) *Atomic Layer Deposition for Semiconductors*; Hwang, C. S. Ed.; Springer: New York, 2014. (d) Atomic Layer Deposition of Nanostructured Materials; Pinna, N., Knez, M. Eds.; Wiley-VCH: Weinheim, Germany, 2012. (e) Johnson, R. W.; Hultqvist, A.; Bent, S. F. *Mater. Today* **2014**, *17*, 236-246.
- (a) Knisley, T. J.; Kalutarage, L. C.; Winter, C. H. *Coord. Chem. Rev.* **2013**, *257*, 3222-3231; (b) Emslie, D. J. H.; Chadha, P.; Price, J. S. *Coord. Chem. Rev.* **2013**, *257*, 3282-3296.
- (a) Klaus, J. W.; Ferro, S. J.; George, S. M. *Thin Solid Films* **2000**, *360*, 145-153; (b) Grubbs, R. K.; Steinmetz, N. J.; George, S. M. *J. Vac. Sci. Technol. B* **2004**, *22*, 1811-1821.
- (a) Kim, S.-H.; Hwang, E.-S.; Kim, B.-M.; Lee, J.-W.; Sun, H.-J.; Hong, T. E.; Kim, J.-K.; Sohn, H.; Kim, J.; Yoon, T.-S. *Electrochem. Solid-State Lett.* **2005**, *8*, C155-C159; (b) Kim, S.-H.; Kwak, N.; Kim, J.; Sohn, H. *J. Electrochem. Soc.* **2006**, *153*, G887-G893.
- Yang, M.; Chung, A.; Yoon, A.; Fang, H.; Zhang, A.; Knepler, C.; Jackson, R.; Byun, J. S.; Mak, A.; Eizenberg, M.; Xi, M.; Kori, M.; Sinha, A. K. In *Conference Proceedings ULSI, XVII*, Conshohocken, PA2002 Materials Research Society: Conshohocken, PA; p 655.
- CRC Handbook of Chemistry and Physics, 92nd Ed.; Haynes, W. M., Ed.; CRC Press, Boca Raton, Florida; 2011-2012; pp 5-80 and 85-89.
- Thompson, D.; Anthis, J. W. Precursors and methods for the atomic layer deposition of manganese. WO2012125439A2, 2012.
- Kalutarage, L. C.; Martin, P. D.; Heeg, M. J.; Winter, C. H. *J. Am. Chem. Soc.* **2013**, *135*, 12588-12591.
- Kalutarage, L. C.; Clendenning, S. B.; Winter, C. H. *ECS Transactions* **2014**, *64*, 147-157.
- Klesko, J. P.; Thrush, C. M.; Winter, C. H. *Chem Mater.* **2015**, *27*, 4918-4921.
- (a) Vidjayacoumar, B.; Emslie, D. J. H.; Clendenning, S. B.; Blackwell, J. M.; Britten, J. F.; Rheingold, A. *Chem. Mater.* **2010**, *22*, 4844-4853; (b) Vidjayacoumar, B.; Ramalingam, V.; Emslie, D. J. H.; Blackwell, J.; Clendenning, S. *Electrochem. Soc. Trans.* **2013**, *50*, 53-66.
- (a) Lim, B. S.; Rahtu, A.; Gordon, R. G. *Nat. Mater.* **2003**, *2*, 749-754; (b) Lim, B. S.; Rahtu, A.; Park, J.-S.; Gordon, R. G. *Inorg. Chem.* **2003**, *42*, 7951-7958.
- Igumenov, I. K.; Semyannikov, P. P.; Trubin, S. V.; Morozova, N. B.; Gelfond, N. V.; Mischenko, A. V.; Norman, J. A. *Surf. Coat. Technol.* **2007**, *201*, 9003-9008.
- Dussarrat, C.; Gatineau, J. *Proc. Electrochem. Soc.* **2005**, *2005-05*, 354-359.
- Utriainen, M.; Kroger-Laukkanen, M.; Johansson, L. S.; Niinistö, L. *Appl. Surf. Sci.* **2000**, *157*, 151-158.
- (a) Senkevich, J. J.; Tang, F.; Rogers, D.; Drotar, J. T.; Jezewski, C.; Lanford, W. A.; Wang, G.; Lu, T. *Chem. Vap. Deposition* **2003**, *9*, 258-264; (b) Ten Eyck, G. A.; Pimanpang, S.; Bakhr, H.; Lu, T.-M.; Wang, G.-C. *Chem. Vap. Deposition* **2006**, *12*, 290-294.
- (a) Maartensson, P.; Carlsson, J. O. *Chem. Vap. Deposition* **1997**, *3*, 45-50; (b) Maartensson, P.; Carlsson, J.-O. *J. Electrochem. Soc.* **1998**, *145*, 2926-2931; (c) Li, Z.; Rahtu, A.; Gordon, R. G. *J. Electrochem. Soc.* **2006**, *153*, C787-C794; (d) Li, Z.; Barry, S. T.; Gordon, R. G. *Inorg. Chem.* **2005**, *44*, 1728-1735.
- Lee, B. H.; Hwang, J. K.; Nam, J. W.; Lee, S. U.; Kim, J. T.; Koo, S.-M.; Baunemann, A.; Fischer, R. A.; Sung, M. M. *Angew. Chem., Int. Ed.* **2009**, *48*, 4536-4539.
- Hierso, J.-C.; Feurer, R.; Kalck, P. *Chem. Mater.* **2000**, *12*, 390-399.
- (a) Aaltonen, T.; Ritala, M.; Sajavaara, T.; Keinonen, J.; Leskelä, M. *Chem. Mater.* **2003**, *15*, 1924-1928; (b) Aaltonen, T.; Ritala, M.; Tung, Y.-L.; Chi, Y.; Arstila, K.; Meinander, K.; Leskelä, M. *J. Mater. Res.* **2004**, *19*, 3353-3358.
- Alkyl complexes of more electropositive metals are typically more reactive towards sigma-bond metathesis reactions: Waterman, R. *Organometallics* **2013**, *32*, 7249-7263.
- (a) Koike, J.; Wada, M. *Appl. Phys. Lett.* **2005**, *87*, 041911; (b) Usui, T.; Nasu, H.; Takahashi, S.; Shimizu, N.; Nishikawa, T.; Yoshimaru, M.; Shibata, H.; Wada, M.; Koike, J. *IEEE Trans. Electron Devices* **2006**, *53*, 2492-2499; (c) Haneda, M.; Iijima, J.; Koike, J. *Appl. Phys. Lett.* **2007**, *90*, 252107; (d) Au, Y.; Lin, Y.; Kim, H.; Beh, E.; Liu, Y.; Gordon, R. G. *J. Electrochem. Soc.* **2010**, *157*, D341-D345; (e) Lozano, J. G.; Lozano-Perez, S.; Bogan, J.; Wang, Y. C.; Brennan, B.; Nellist, P. D.; Hughes, G. *Appl. Phys. Lett.* **2011**, *98*, 123112.
- Hartwing, J., *Organotransition Metal Chemistry: From Bonding to Catalysis*. University Science Books: Sausalito, California, 2010.
- (a) Ozin, G. A.; McCaffrey, J. G. *J. Am. Chem. Soc.* **1984**, *106*, 807-809; (b) Wang, X.; Andrews, L. *J. Phys. Chem. A* **2003**, *107*, 4081-4091.
- Beerman, C.; Clauss, K. *Angew. Chem.* **1959**, *71*, 627.

28. (a) Andersen, R. A.; Carmona-Guzman, E.; Mertis, K.; Sigurdson, E.; Wilkinson, G. *J. Organomet. Chem.* **1975**, *99*, C19-C20; (b) Andersen, R. A.; Carmona-Guzman, E.; Gibson, J. F.; Wilkinson, G. *J. Chem. Soc., Dalton Trans.* **1976**, 2204-2211.
29. Bochmann, M.; Wilkinson, G.; Young, G. B. *J. Chem. Soc., Dalton Trans.* **1980**, 1879-1887.
30. Personal communication (ref. 6) within reference 28b.
31. Campora, J.; Palma, P.; Perez, C. M.; Rodriguez-Delgado, A.; Alvarez, E.; Gutierrez-Puebla, E. *Organometallics* **2010**, *29*, 2960-2970.
32. Manzer, L. E.; Guggenberger, L. J. *J. Organomet. Chem.* **1977**, *139*, C34-C38.
33. Andersen, R. A.; Berg, D. J.; Fernholt, L.; Faegri, K., Jr.; Green, J. C.; Haaland, A.; Lappert, M. F.; Leung, W. P.; Rypdal, K. *Acta Chem. Scand., Ser. A* **1988**, *A42*, 554-562.
34. Buttrus, N. H.; Eaborn, C.; Hitchcock, P. B.; Smith, J. D.; Sullivan, A. C. *J. Chem. Soc., Chem. Commun.* **1985**, 1380-1381.
35. Al-Juaid, S. S.; Eaborn, C.; El-Hamrui, S. M.; Hitchcock, P. B.; Smith, J. D.; Sozerli Can, S. E. *J. Organomet. Chem.* **2002**, *649*, 121-127.
36. (a) Davis, J. I.; Howard, C. G.; Skapski, A. C.; Wilkinson, G. *J. Chem. Soc., Chem. Commun.* **1982**, 1077-1078; (b) Howard, C. G.; Girolami, G. S.; Wilkinson, G.; Thornton-Pett, M.; Hursthouse, M. B. *J. Chem. Soc., Dalton Trans.* **1983**, 2631-2637.
37. Howard, C. G.; Wilkinson, G.; Thornton-Pett, M.; Hursthouse, M. B. *J. Chem. Soc., Dalton Trans.* **1983**, 2025-2030.
38. (a) Girolami, G. S.; Wilkinson, G.; Galas, A. M. R.; Thornton-Pett, M.; Hursthouse, M. B. *J. Chem. Soc., Dalton Trans.* **1985**, 1339-1348; (b) Hitchcock, P. B.; Lappert, M. F.; Leung, W. P.; Buttrus, N. H. *J. Organomet. Chem.* **1990**, *394*, 57-67.
39. Alberola, A.; Blair, V. L.; Carrella, L. M.; Clegg, W.; Kennedy, A. R.; Klett, J.; Mulvey, R. E.; Newton, S.; Rentschler, E.; Russo, L. *Organometallics* **2009**, *28*, 2112-2118.
40. Riollet, V.; Coperet, C.; Basset, J.-M.; Rousset, L.; Bouchu, D.; Grosvalet, L.; Perrin, M. *Angew. Chem., Int. Ed.* **2002**, *41*, 3025-3027.
41. Bart, S. C.; Hawrelak, E. J.; Schmisser, A. K.; Lobkovsky, E.; Chirik, P. J. *Organometallics* **2004**, *23*, 237-246.
42. Crewdson, P.; Gambarotta, S.; Yap, G. P. A.; Thompson, L. K. *Inorg. Chem.* **2003**, *42*, 8579-8584.
43. Blair, V. L.; Clegg, W.; Conway, B.; Hevia, E.; Kennedy, A.; Klett, J.; Mulvey, R. E.; Russo, L. *Chem. - Eur. J.* **2008**, *14*, 65-72.
44. Kennedy, A. R.; Klett, J.; Mulvey, R. E.; Robertson, S. D. *Eur. J. Inorg. Chem.* **2011**, *2011*, 4675-4679.
45. Girolami, G. S.; Howard, C. G.; Wilkinson, G.; Dawes, H. M.; Thornton-Pett, M.; Motevalli, M.; Hursthouse, M. B. *J. Chem. Soc., Dalton Trans.* **1985**, 921-929.
46. Complex **1** has previously been characterized crystallographically; refs. 28b and 39.
47. Andersen, R. A.; Haaland, A.; Rypdal, K.; Volden, H. V. *J. Chem. Soc., Chem. Commun.* **1985**, 1807-1808.
48. Meier, R. M.; Hanusa, T. P. In *Structural Organomanganese Chemistry*, John Wiley & Sons Ltd., 2011, pp 43-169.
49. CRC Handbook of Chemistry and Physics, 95th Ed.; Haynes, W. M., Ed.; CRC Press, Boca Raton, Florida; 2014-2015; Section 9: Molecular Structure and Spectroscopy-Atomic Radii of the Elements.
50. (a) Oberteuffer, J. A.; Ibers, J. A. *Acta Crystallogr., Sect. B* **1970**, *26*, 1499-1504; (b) Preston, G. D. *Philos. Mag.* **1928**, *5*, 1207-1225; (c) Haglund, J.; Fernandez Guillermet, F.; Grimvall, G.; Koring, M. *Phys. Rev. B.* **1993**, *48*, 11685-11691.
51. Dunitz, J. D., *Perspectives in Structural Chemistry*. John Wiley and Sons: New York, 1968; Vol. II.
52. Hilderbrandt, R. L.; Wieser, J. D.; Montgomery, L. K. *J. Am. Chem. Soc.* **1973**, *95*, 8598.
53. Dumke, A. C.; Pape, T.; Kösters, J.; Feldmann, K.-O.; Schulte to Brinke, C.; Hahn, F. E. *Organometallics* **2013**, *32*, 289-299.
54. Attempts to determine whether the dimeric structure of complex **4** (Figure 3) remained intact in solution or dissociated into monometallic species using DOSY NMR failed due to very short T_1 relaxation times (the average for the three signals in complex **4** is 0.282 ms at 0.03 g/mL).
55. Xu, Z.; Thompson, L. K.; Waldmann, O. *MAGMUN4.1*.
56. (a) Evans, D. F. *J. Chem. Soc.* **1959**, 2003-2005; (b) Schubert, E. M. *J. Chem. Educ.* **1992**, *69*, 62.
57. For **5**, four equivalents of SiMe₄ were observed after the intermediate (**3**) had reacted with excess H₂ at 120 °C for 12 h.
58. Complex **5** slowly decomposed to **3** at 120 °C in solution. However, this decomposition proceeded much more slowly than the reaction to form **3** in the presence of H₂.
59. NMR signals for free dmpm were shifted by 0.05-0.1 ppm (¹H NMR) and 1-3 ppm (³¹P NMR) relative to a reference sample.
60. A small amount of an unidentified phosphorous-containing product was observed in the reaction of **3** with ZnEt₂ at 60 °C. This product was not observed in the reaction of **5** with ZnEt₂, most likely due to milder reaction conditions.
61. Nakagawa, Y.; Hori, T. *Trans. Jpn. Inst. Met.* **1972**, *13*, 165-170.
62. (a) Zhu, Z.; Wright, R. J.; Olmstead, M. M.; Rivard, E.; Brynda, M.; Power, P. P. *Angew. Chem., Int. Ed.* **2006**, *45*, 5807-5810; (b) Zhu, Z.; Brynda, M.; Wright, R. J.; Fischer, R. C.; Merrill, W. A.; Rivard, E.; Wolf, R.; Fettinger, J. C.; Olmstead, M. M.; Power, P. P. *J. Am. Chem. Soc.* **2007**, *129*, 10847-10857.
63. Zhu, Z.; Fettinger, J. C.; Olmstead, M. M.; Power, P. P. *Organometallics* **2009**, *28*, 2091-2095.
64. Greene, T. M.; Andrews, L.; Downs, A. J. *J. Am. Chem. Soc.* **1995**, *117*, 8180-8187.
65. Flory, M. A.; Apponi, A. J.; Zack, L. N.; Ziurys, L. M. *J. Am. Chem. Soc.* **2010**, *132*, 17186-17192.
66. ZnH₂ is reported to decompose to Zn and H₂ at 90 °C: Ashby, E. C.; Watkins, J. J. *Inorg. Synth.* **1977**, *17*, 6-9.
67. Chadha, P.; Emslie, D. J. H.; Jenkins, H. A. *Organometallics* **2014**, *33*, 1467-1474.
68. Burger, B. J.; Bercaw, J. E., *Vacuum Line Techniques for Handling Air-Sensitive Organometallic Compounds*. In *Experimental Organometallic Chemistry - A Practicum in Synthesis and Characterization*, American Chemical Society: Washington D.C., 1987; Vol. 357, pp 79-98.
69. Andersen, R. A.; Wilkinson, G. *Inorg. Synth.* **1979**, *19*, 262-264.
70. Fulmer, G. R.; Miller, A. J. M.; Sherden, N. H.; Gottlieb, H. E.; Nudelman, A.; Stoltz, B. M.; Bercaw, J. E.; Goldberg, K. I. *Organometallics* **2010**, *29*, 2176-2179.
71. Sheldrick, G. M. *Acta Crystallogr., Sect. A* **2008**, *64*, 112-122.

Insert Table of Contents artwork here

